

RESONANCE RAMAN SPECTROSCOPY OF MANGANESE(III)

ETIOPORPHYRIN I: THEORY AND EXPERIMENT

A THESIS

Presented to

The Faculty of the Division of Graduate

Studies and Research

By

John Allen Shelnutt

In Partial Fulfillment

of the Requirements for the Degree

Doctor of Philosophy

in the School of Physics

Georgia Institute of Technology

November, 1975

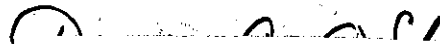
Copyright, 1975 by John Allen Shelnutt

Original Page Numbering Retained.

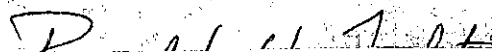
RESONANCE RAMAN SPECTROSCOPY OF MANGANESE(III)

ETIOPORPHYRIN I: THEORY AND EXPERIMENT

Approved:



Donald C. O'Shea, Chairman



Ronald H. Felton



Ronald F. Fox

Date approved by Chairman:

11/14/75

ACKNOWLEDGEMENTS

The author wishes to express appreciation to Dr. D. C. O'Shea for his support and effort as thesis advisor.

I would also like to extend thanks to my reading committee, especially Dr. R. H. Felton, whose continued interest and assistance in my research provided the motivation necessary to complete the investigation.

Special thanks is extended to Mr. Jim Martin for his friendship throughout my graduate career.

Most of all I would like to thank Rebecca, friend and lover, and my son, Judson, for their love and understanding which made the endeavor possible.

TABLE OF CONTENTS

	Page
ACKNOWLEDGEMENTS	ii
LIST OF TABLES	v
LIST OF ILLUSTRATIONS	vi
SUMMARY	viii
Chapter	
I. INTRODUCTION	1
Review of the Problem	1
Organization of the Thesis	5
II. THEORY	7
The Theory of Raman Intensities	7
The Raman Scattering Tensor	9
Structure and Symmetry of Metalloporphyrins	17
Metalloporphyrin Excited States	18
Vibronic Coupling in Metalloporphyrins	20
Resonance Raman Scattering in Metalloporphyrins	24
Frequency Dependence of Raman Intensities in	24
Metalloporphyrins	29
Inclusion of Charge Transfer States	35
III. EXPERIMENTAL	44
The Samples	44
The Raman Scattering Apparatus	45
Methods	51
IV. RESULTS	53
Raman Spectra	54
Excitation Profiles	58
V. DISCUSSION AND CONCLUSIONS	64
Introduction	64
Electronic Assignments for Bands III and IV	65
Electronic Assignments for Bands V	66

TABLE OF CONTENTS (Continued)

Chapter	Page
Mn(III)TPPX Resonance Raman Data.	68
Band V and V_a Excitation Profiles	69
Vibronic Coupling by Totally Symmetric Modes.	70
APPENDIX	76
Introduction.	76
Perturbation Theory	76
The Interaction Matrix Elements	77
The Transition Probabilities.	79
The Raman Scattering Tensor and Transition Rates.	79
BIBLIOGRAPHY	82
VITA	86

LIST OF TABLES

Table	Page
1. Symmetries Required to Mix States (Before CI) by One-Electron Perturbations	39

LIST OF ILLUSTRATIONS

Figure	Page
1. Absorption Spectrum of a Typical Metalloporphyrin: Copper (II) Octaethylporphyrin in n-Hexane at Room Temperature . . .	2
2. Manganese(III) Etioporphyrin I Thiocyanate Absorption Spectrum in Methylene Chloride.	3
3. Structure of Manganese(III) Etioporphyrin I	19
4. Ground and Excited State (a) Configurations and (b) Molecular States Before and After Configuration Interaction .	21
5. Raman Intensity as a Function of Exciting Frequency: B Term Only	32
6. Manganese(III) Porphyrin Molecular Orbital Energy Levels for the Ground State Including Metal Orbitals.	36
7. Raman Scattering Apparatus.	46
8. Standard Raman Scattering Arrangement: 90° Scattering Geometry.	48
9. Resonance Raman Spectrum of Manganese(III) Etioporphyrin I Chloride in KBr	54
10. Resonance Raman Spectrum of Manganese(III) Etioporphyrin I Thiocyanate in Carbon Disulfide	55
11. Resonance Raman Spectrum of Manganese(III) Etioporphyrin I Iodide in Carbon Disulfide.	56
12. Resonance Raman Spectrum of Chromium(III) Tetraphenyl Porphyrin in Methylene Chloride	57
13. Manganese(III) Etioporphyrin I Chloride Excitation Profile and Absorption Spectrum in KBr.	59
14. Manganese(III) Etioporphyrin I Thiocyanate Excitation Profiles and Absorption Spectrum in Carbon Disulfide.	60
15. Manganese(III) Etioporphyrin I Thiocyanate Excitation Profiles and Absorption Spectrum in CHCl_3 or CDCl_3	61

LIST OF ILLUSTRATIONS (Continued)

Figure	Page
16. Manganese(III) Etioporphyrin I Iodide Excitation Profile and Absorption Spectrum in Methylene Chloride	63
17. Calculated Raman Intensity When Only B and D Terms Contribute.	71
18. Porphyrin Molecular Orbitals.	74

SUMMARY

Resonance Raman spectra of manganese(III) etioporphyrin I complexes have been obtained with laser excitation in the regions of the Bands III and IV, and Bands V and V_a of the atypical visible absorption spectra of these metalloporphyrins. Excitation profiles in the latter region are interpreted as indicating non-adiabatic coupling between V and V_a as well as vibronic activity of some totally symmetric modes. The Raman data support assignment of Bands III and IV to the 0-0 and 0-1 components of the Q band. Although Bands V and V_a are assigned to a charge transfer transition mixed with the main $\pi \rightarrow \pi^*$ transition, no selective enhancement of low frequency metal-ligand vibrations attributable to the charge transfer contribution of Band V was observed.

CHAPTER I

INTRODUCTION

Review of the Problem

Resonance Raman spectroscopy has been used as a tool for probing the electronic and vibrational structure which gives rise to the atypical absorption spectrum of hyperporphyrins--in particular, Mn(III) etioporphyrin complexes. The typical electronic absorption spectrum of a metalloporphyrin (Figure 1) displays an intense B (Soret) band at $24,000 \text{ cm}^{-1}$ and a weaker Q band at $18,000 \text{ cm}^{-1}$.^{1,2} A vibrationally induced absorption band is observed on the high energy side of the Q band. The electronic structure which produces these bands has been discussed by Gouterman^{1,3,4} and others.^{2,4,6} On the other hand the optical absorption spectrum of manganese(III) porphyrins (Figure 2) is atypical in that two relatively strong "Soret-like" absorptions are found at $21,000 \text{ cm}^{-1}$ (Band V) and at $28,000 \text{ cm}^{-1}$ (Band VI). Additional weaker bands are also observed in the $12,000$ to $15,000 \text{ cm}^{-1}$ region. The electronic origin of the "extra" bands is not well understood in manganese(III) porphyrins or in the closely related and biologically relevant Fe(III) porphyrins, and for this reason laser Raman studies were undertaken.

Since Band V resides in a spectral region accessible to argon and krypton ion laser irradiation and Bands III and IV are accessible to dye laser excitation frequencies, resonance Raman excitation profiles

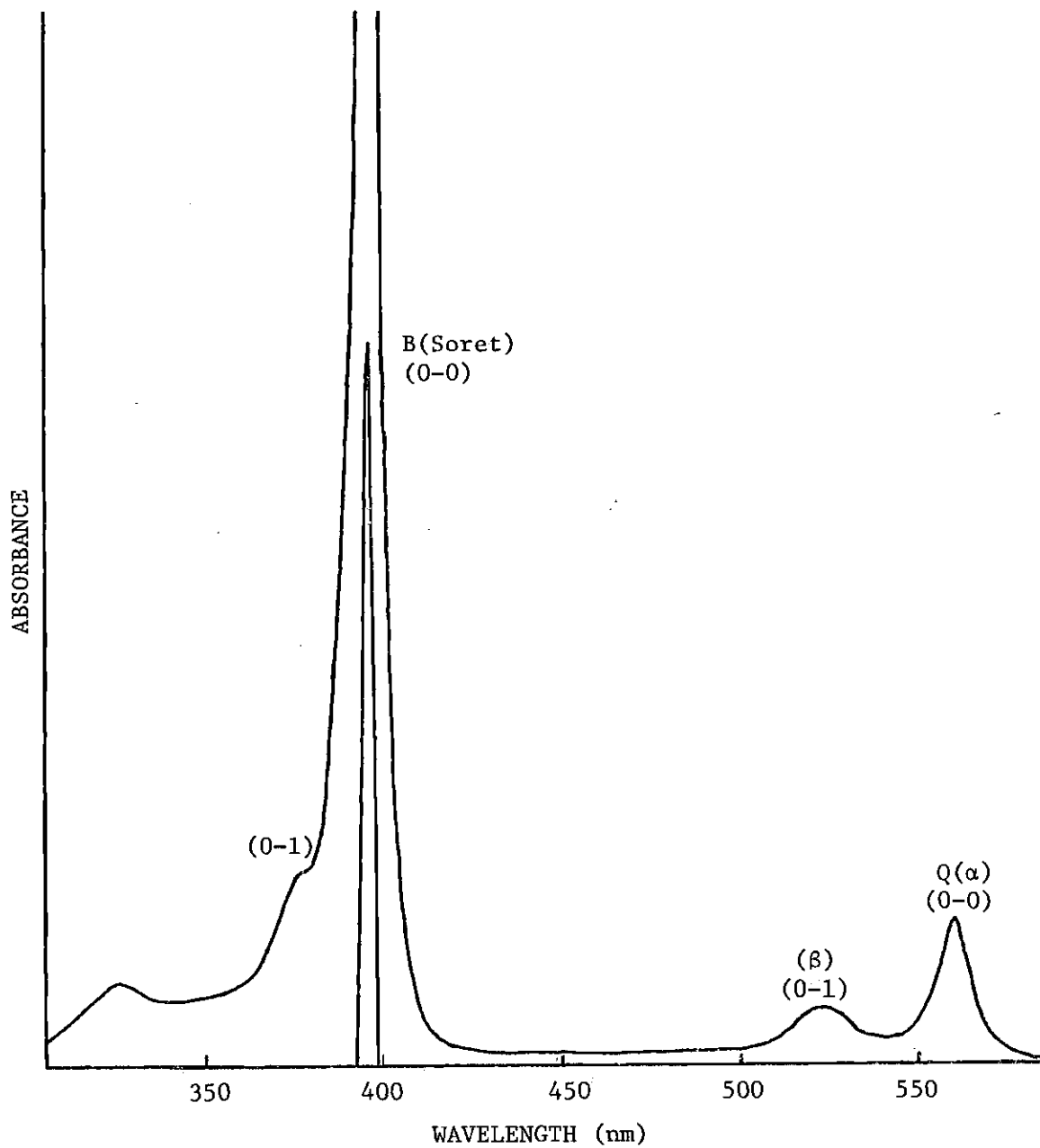


Figure 1. Absorption Spectrum of a Typical Metalloporphyrin: Copper(II) Octaethylporphyrin in n-Hexane at Room Temperature

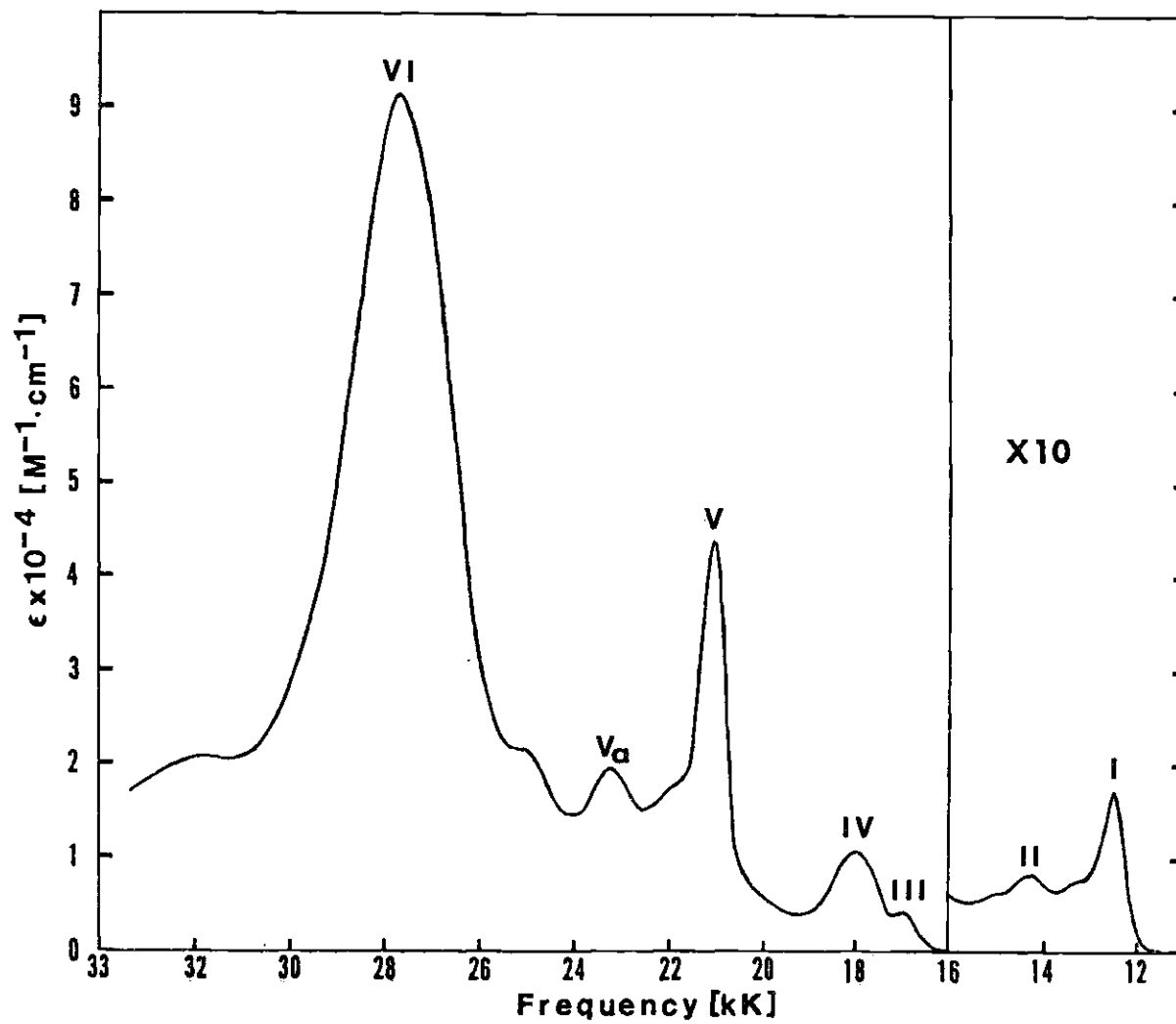


Figure 2. Manganese(III) Etioporphyrin I Thiocyanate Absorption Spectrum in Methylene Chloride

can be employed to elucidate the nature of the excited states in Mn(III) porphyrins. Excitation profiles exhibit the dependence of scattered light intensity for a porphyrin Raman line as a function of the exciting laser frequency. Recently, Gaughan et al.⁷ obtained resonance Raman spectra of Mn(III) tetraphenyl porphyrin (Mn(III)TPP) halide complexes. Their data is comparable to the present results for Mn(III) etioporphrin I (Mn(III)EtioI)X where $X^- = Cl^-, I^-, \text{ and } SCN^-$.

In recent reviews, Boucher^{8,9} has suggested that Band V, and either Band III or IV are charge transfer transitions from porphyrin π -orbitals to metal d_{π} orbitals. This conclusion is based primarily upon changes in Band V of the optical absorption spectrum as the axial anion is changed. (See Figure 2'.) Gaughan et al. interpreted their data in favor of a charge transfer assignment for Band V based on its unusually rich low frequency Raman spectrum.

Initially, we too hoped to observe selective enhancement of low frequency, metal-ligand mode Raman intensity upon excitation into Band V, since assignment to a charge transfer transition has been proposed. However, examination of the scattering tensor with charge transfer states included (Chapter II) shows that upon excitation into a charge transfer band, selective enhancement can occur for only those vibrational modes containing appreciable metal-nitrogen (Mn-N) character. Further detailed theoretical considerations indicate selective enhancement of low frequency metal-ligand modes does not occur in manganese(III) porphyrins upon excitation in Band V; furthermore, should weak selective enhancement of metal-ligand vibrations actually occur, it would be

obscured by the strong Frank-Condon mode enhancement in Band V which is independent of charge transfer character.

Organization of the Thesis

To outline the contents of the thesis and to emphasize the more important results of the study, the content of each chapter is described briefly. In Chapter II the theory of Raman intensities is reviewed and a derivation of the resonance Raman scattering tensor, including non-adiabatic coupling of the crude Born-Oppenheimer states, is presented. The expression (equation (16)) is essentially the one first derived by Mingardi and Siebrand in 1975.¹⁰ Emphasis here is on the nonadiabatic coupling term (20), since it is essential to understanding the unusual behavior of excitation profiles in Band V of manganese(III) porphyrins. Chapter II also contains introductory sections concerning the chemical and electronic structure of typical metalloporphyrins, and, in addition, three sections are devoted to the application of the scattering tensor (16) to vibronic borrowing of intensity in the absorption spectrum and resonance Raman scattering in typical metalloporphyrins. Finally, the model proposed for including the charge transfer states in metalloporphyrins is presented, and the implications of this model for resonance Raman scattering in these systems are discussed. In Chapter III the details of sample preparation, description of the Raman scattering apparatus, and experimental techniques are presented. In Chapter IV typical Raman spectra are displayed and their qualitative features noted; however, emphasis here is on the excitation profiles provided by the Raman spectra obtained at different laser exciting frequencies.

In Chapter V the results of the resonance Raman study are discussed, and emphasis is on three conclusions. (1) A consistent interpretation of hyperporphyrin absorption spectra is arrived at and is based on electronic band assignments suggested by the resonance Raman spectra of Mn(III) and Cr(III) porphyrins, in conjunction with the conclusions of Gouterman et al.¹¹ on Cr(III) porphyrin emission and absorption spectra. (2) The importance of nonadiabatic coupling terms in the Raman tensor in interpreting excitation profiles of Mn(III) porphyrins is shown, and (3) evidence based on the Band V excitation profiles indicates vibronic activity of some totally symmetric modes.

CHAPTER II

THEORY

The Theory of Raman Intensities

The semi-classical theory of scattering of light by a single particle based on second order perturbation theory was presented in 1925 by Kramers and Heisenberg,¹² and later verified by Dirac¹³ on the basis of radiation-field theory. The problem of scattering of light by polyatomic molecules was considered by Van Vleck,¹⁴ who derived selection rules for the vibrational Raman effect, and Placzek,¹⁵ who demonstrated that the intensity of molecular Raman scattering arises from the dependence of the ground state polarizability on the nuclear vibrations. Albrecht^{16,17} extended the theory to include vibronic interactions by using the crude Born-Oppenheimer states as a basis and expanding¹⁸ (Herzberg-Teller expansion) the electronic integrals to first order in the normal coordinates. These theories of Raman intensity do not apply when the energy of the light impinging on the molecule is at or near resonance with an electronic transition.

It is clear that any theory of resonance transformation of light which is based on second order time dependent perturbation theory, must include damping,^{19,20} otherwise the expression for the transition probabilities will contain singularities due to the energy denominators. Inclusion of damping of states in transition probabilities was first treated by Wigner and Weisskopf,²¹ and subsequently by Heitler and Ma,²²

or by others^{23,24} using the resolvent formalism.²⁵ Sushchinskii,²⁶ employing an antihermitian damping operator which represents an additive part of the interaction hamiltonian, arrived at the same results obtained by the method of Heitler and Ma. Although the method is claimed to be unphysical because of the antihermitian property of the damping hamiltonian,¹⁹ this objection can be removed, since the antihermitian damping hamiltonian can be shown²⁷ to arise naturally from a hermitian hamiltonian describing a randomly fluctuating interaction, say an interaction with the environment. Using the theory of multiplicative stochastic processes²⁸ the transition probabilities for transformation of light by polyatomic molecules (to second order in the perturbation theory) can be obtained with damping due to the random interaction included. Here, the U-matrix formulation (as opposed to the S-matrix formulation) of the perturbation theory is used so as to include transient effects which may be important near resonance.²⁹ The result is formally identical to Sushchinskii's expressions; however, now the damping coefficients are defined in terms of the statistical properties of the fluctuating interaction hamiltonian. It can be shown^{24,30} that S-matrix and U-matrix theories give identical results for excitation into a sufficiently broad quasicontinuum consisting of overlapping vibronic bands.¹⁰ This situation is realized for excitation in the visible for metalloporphyrins at room temperature; consequently, the transition rate, (equation (A-17)), whose derivation is outlined in the Appendix provides the fundamental expression from which intensities for resonance Raman scattering are calculated in terms of the Raman scattering tensor defined by equation (1) below.

The Raman Scattering Tensor

The applicability of the expressions for resonance Raman intensities to metalloporphyrins rests on the approximations which are made. The expressions presented below, were first derived by Mingardi and Siebrand¹⁰ and are rederived in order to indicate the approximations inherent in their theory. Further approximations are made here, and their significance discussed. The expression for the Raman scattering tensor which results will be used in a following section to arrive at the predicted frequency dependence of Raman line intensities for typical metalloporphyrins.

We begin with the scattering tensor, equation (A-18) in the Appendix,

$$(\alpha_{\rho\sigma})_{n'n} = \sum_i \left[\frac{\langle n' | R_{\rho} | i \rangle \langle i | R_{\sigma} | n \rangle}{E_i - E_n + h\nu - i\Gamma_i} + \frac{\langle n' | R_{\sigma} | i \rangle \langle i | R_{\rho} | n \rangle}{E_i - E_n - h\nu - i\Gamma_i} \right] \quad (1)$$

where E_i and Γ_i are the energy and damping coefficient of the exact molecular eigenstate $|i\rangle$, R_{ρ} is the ρ^{th} component of the electric dipole operator, and the summation is over all molecular states except n and n' . The subscript $\rho = X, Y, Z$, the coordinate axes in the molecular frame.

Since the exact molecular eigenstates are not available, suitable approximate states must be obtained. The adiabatic Born-Oppenheimer states are defined by,³¹

$$|iu\rangle' \equiv |i\rangle|u\rangle \quad (2)$$

where the electronic state $|i\rangle$ depends on the electronic coordinates q and the nuclear coordinates Q ; where the vibrational state $|u\rangle$ depends

on the nuclear coordinates only.

If the nuclei were fixed (infinitely massive), then the electrons would satisfy the Schrodinger equation,

$$H_e |i\rangle = E_i(Q) |i\rangle \quad (3)$$

where $H_e \equiv H_{\text{molecule}} - T_N$ is the the electronic hamiltonian, and includes the nuclear-nuclear, nuclear-electronic, and electronic repulsion potentials (V_{NN} , V_{Ne} , and V_{ee} , respectively), and T_N is the nuclear kinetic energy operator. The electronic states $|i\rangle$, satisfying (3), will depend parametrically on the nuclear coordinates through V_{Ne} and V_{NN} , with V_{NN} entering the electronic Schrodinger equation as an additive constant. With (2) and (3), the exact Schrodinger equation for the molecule becomes,

$$\{T_N(|i\rangle|u\rangle) - |i\rangle T_N |u\rangle\} + |i\rangle [T_N + E_i(Q)] |u\rangle = E_{iu} |i\rangle |u\rangle \quad (4)$$

where the term $|i\rangle T_N |u\rangle$ is added and subtracted on the left hand side. The first term in the curly brackets gives three terms bilinear in the derivatives with respect to the nuclear coordinates--one of these terms exactly cancels the second term in the curly brackets. In a first approximation, the two remaining terms can be neglected because of the smallness of the amplitudes of the nuclear motion in comparison to the internuclear distances,³¹ and (4) provides a Schrodinger equation for the vibrational states $|u\rangle$ and the energy, E_{iu} , of the Born-Oppenheimer state, $|iu\rangle$,

$$[T_N + E_i(Q)] |u\rangle = E_{iu} |u\rangle \quad (5)$$

This says that the nuclei move in the effective potential provided by

the electronic energy, $E_i(Q)$, which includes V_{NN} . Conventionally, (5) is solved by approximating $E_i(Q)$ with a harmonic potential and transforming to the normal mode coordinates. The vibrational states are then products of the individual normal mode state functions, i.e., $|u\rangle = \prod_K |u_K\rangle$ where the u_K are the quantum numbers of the individual harmonic oscillator wave functions, and the vibrational energies are given by $\epsilon_u = \sum_K \hbar \omega_K u_K$.

The adiabatic Born-Oppenheimer approximation relies on the difference in response times of the electrons and nuclei due to the great disparity in the electronic and nuclear masses. Solution of (3) provides the electronic energies and states under the physically reasonable assumption that the nuclei are fixed, and (5) says that the nuclei move in the effective potential which is the electronic energy of the relevant state as a function of the nuclear coordinates.

An improved approximation for the molecular states includes the operator which couples the adiabatic Born-Oppenheimer states to first order in the perturbation. Making the harmonic oscillator approximation for the vibrational states and transforming to the normal coordinates, Q_K , the molecular eigenstates can be approximated by

$$|iu\rangle = |i\rangle|u\rangle + \sum_j \sum_x \frac{\langle x|\langle j|[T_N(|i\rangle|u\rangle) - |i\rangle T_N|u\rangle]}{E_{iu} - E_{jx}} |j\rangle|x\rangle \quad (6)$$

where the matrix element is given by, (7)

$$\langle x|\langle j|[T_N(|i\rangle|u\rangle) - |i\rangle T_N|u\rangle] = \quad (7)$$

$$\begin{aligned}
&= - \sum_{\mathbf{K}} \frac{\hbar^2}{2\mu_{i\mathbf{K}}} \left[\langle j | \langle \mathbf{x} | \frac{\partial^2}{\partial Q_{\mathbf{K}}^2} (|i\rangle |u\rangle) - \langle j | \langle \mathbf{x} | \frac{\partial^2}{\partial Q_{\mathbf{K}}^2} |u\rangle |i\rangle \right] \\
&= - \hbar^2 \sum_{\mathbf{K}} \frac{1}{\mu_{i\mathbf{K}}} \left[\frac{1}{2} \langle \mathbf{x} | \langle j | \frac{\partial^2}{\partial Q_{\mathbf{K}}^2} |i\rangle |u\rangle + \langle \mathbf{x} | \langle j | \frac{\partial}{\partial Q_{\mathbf{K}}} |i\rangle \frac{\partial}{\partial Q_{\mathbf{K}}} |u\rangle \right]
\end{aligned}$$

where $\mu_{i\mathbf{K}}$ is the reduced mass associated with the \mathbf{K}^{th} mode and the potential curve in the i^{th} electronic state. If the electronic matrix elements are expanded about the symmetric equilibrium positions, $Q_{\mathbf{K}} = 0$ for all electronic ground state normal modes, we obtain,

$$\begin{aligned}
\langle \mathbf{x} | \langle j | [T_N (|i\rangle |u\rangle) - |i\rangle T_N |u\rangle] &= \hbar^2 \sum_{\mathbf{K}} \frac{1}{\mu_{i\mathbf{K}}} \left\{ \frac{1}{2} \langle j | \frac{\partial^2}{\partial Q_{\mathbf{K}}^2} |i\rangle \langle \mathbf{x} | u \rangle \right. & (8) \\
&+ \langle j | \frac{\partial}{\partial Q_{\mathbf{K}}} |i\rangle \langle \mathbf{x} | \frac{\partial}{\partial Q_{\mathbf{K}}} |u\rangle + \frac{1}{2} \sum_{\mathbf{L}} \left(\frac{\partial}{\partial Q_{\mathbf{K}}} \langle j | \frac{\partial^2}{\partial Q_{\mathbf{K}}^2} |i\rangle \right)_0 \langle \mathbf{x} | Q_{\mathbf{L}} |u\rangle \\
&+ \left. \sum_{\mathbf{L}} \left(\frac{\partial}{\partial Q_{\mathbf{L}}} \langle j | \frac{\partial}{\partial Q_{\mathbf{K}}} |i\rangle \right)_0 \langle \mathbf{x} | Q_{\mathbf{L}} \frac{\partial}{\partial Q_{\mathbf{K}}} |u\rangle + \dots \right\} \\
&= - \frac{\hbar^2}{2} \sum_{\mathbf{K}} \frac{1}{\mu_{i\mathbf{K}}} \left\{ \left[\sum_{\ell} \langle j | \frac{\partial}{\partial Q_{\mathbf{K}}} | \ell \rangle \langle \ell | \frac{\partial}{\partial Q_{\mathbf{K}}} |i\rangle_0 + \left(\frac{\partial}{\partial Q_{\mathbf{K}}} \langle j | \frac{\partial}{\partial Q_{\mathbf{K}}} |i\rangle \right)_0 \right] \langle \mathbf{x} | u \rangle \right. \\
&+ 2 \langle j | \frac{\partial}{\partial Q_{\mathbf{K}}} |i\rangle \langle \mathbf{x} | \frac{\partial}{\partial Q_{\mathbf{K}}} |u\rangle \\
&+ \left. \sum_{\ell} \sum_{\mathbf{L}} \left[\langle j | \frac{\partial}{\partial Q_{\mathbf{K}}} | \ell \rangle \langle \ell | \frac{\partial}{\partial Q_{\mathbf{L}}} |i\rangle_0 \right. \right.
\end{aligned}$$

$$= \left\langle j \left| \frac{\partial}{\partial Q_L} \right| l \right\rangle_0 \left\langle l \left| \frac{\partial}{\partial Q_K} \right| i \right\rangle_0 \left\langle x \left| Q_L \frac{\partial}{\partial Q_K} \right| u \right\rangle \quad (8)$$

The second equality follows on expressing the electronic matrix in terms of elements like $\langle l \left| \frac{\partial}{\partial Q_K} \right| m \rangle_0$ as far as possible,³² and on neglecting electronic matrix elements containing higher than second order derivatives with respect to the nuclear coordinates. The subscript zero indicates that the matrix elements are to be evaluated at $Q = 0$.

Keeping only the term linear in $\langle j \left| \frac{\partial}{\partial Q_K} \right| i \rangle_0$ in (8), and expanding the electronic states, $|i\rangle$, about $Q = 0$ we have to first order in $\langle j \left| \frac{\partial}{\partial Q_K} \right| i \rangle_0$ for (6),

$$|iu\rangle = |i\rangle_0 |u\rangle + \sum_j \sum_k \langle j \left| \frac{\partial}{\partial Q_K} \right| i \rangle_0 |j\rangle_0 Q_K |u\rangle \quad (9)$$

$$- \hbar^2 \sum_j \sum_x \sum_K \frac{1}{\mu_{iK}} \frac{\langle j \left| \frac{\partial}{\partial Q_K} \right| i \rangle_0 \langle x \left| \frac{\partial}{\partial Q_K} \right| u \rangle}{E_{iu} - E_{jx}} |j\rangle_0 |x\rangle, \quad (10)$$

and

$$\langle iu| = \langle i|_0 \langle u| - \sum_j \sum_K \langle i \left| \frac{\partial}{\partial Q_K} \right| j \rangle_0 \langle u| Q_K \langle j|_0 \quad (10)$$

$$- \hbar^2 \sum_j \sum_x \sum_K \frac{1}{\mu_{jK}} \frac{\langle i \left| \frac{\partial}{\partial Q_K} \right| j \rangle_0 \langle u \left| \frac{\partial}{\partial Q_K} \right| x \rangle}{E_{iu} - E_{jx}} \langle x| \langle j|_0 \quad (11)$$

since $\frac{\partial}{\partial Q_K}$ is an anti-hermitian operator.

To obtain the electronic matrix elements appearing in (9) and

(10) we need the electronic states $|i\rangle$. These are given by (3), which can be solved in an approximate manner by expanding the electronic-nuclear potential about $Q=0$ and by using the linear term, $\sum_K \left(\frac{\partial V_{Ne}}{\partial Q_K}\right)_{Q=0} Q_K$, as the perturbation. In employing the conventional treatment here, we differ from Mingardi and Siebrand.¹⁰ In terms of the state $|i_0\rangle$ defined by

$$H_e(Q=0)|i_0\rangle = E_i^0|i_0\rangle, \quad (11)$$

the electronic state $|i\rangle$ to first order (Herzberg-Teller) is,

$$|i\rangle = |i_0\rangle + \sum_{j \neq i} \sum_K \frac{h_{ji}^K}{E_i^0 - E_j^0} Q_K |j_0\rangle \quad (12)$$

where $h_{ji}^K = \langle j_0 | \left(\frac{\partial V_{Ne}}{\partial Q_K}\right)_0 | i_0 \rangle$, and,

$$\left(\frac{\partial V_{Ne}}{\partial Q_K}\right)_0 = \sum_m h_{(m)}^K = \sum_m \delta_{jm} \left[\sum_\lambda \left[\frac{\partial \left(\frac{-eZ_\lambda}{r_{m\lambda}} \right)}{\partial Q_K} \right]_{Q=0} \right] |i_0\rangle \quad (13)$$

where $r_{m\lambda}$ is the distance between m^{th} electron and the λ^{th} nucleus with charge $Z_\lambda |e|$. Using the states (12) the electronic matrix element

$$\begin{aligned} \langle j | \frac{\partial}{\partial Q_K} | i \rangle &= \left(\frac{h_{ji}^K}{E_i^0 - E_j^0} + \text{linear and higher order terms in the nuclear coordinates} \right)_{Q=0} \quad (14) \\ &= \frac{h_{ji}^K}{E_i^0 - E_j^0} = - \langle i | \frac{\partial}{\partial Q_K} | j \rangle \quad (i \neq j) \end{aligned}$$

From (14) it is obvious that only the second term in (8) will be linear in h_{ji}^K , so that (9) and (10) include all terms linear in h_{ji}^K .

With (14) substituted into (9) and (10), and the harmonic oscillator identity,¹⁰

$$\begin{aligned} \langle x | \frac{\partial}{\partial Q_K} | u \rangle &= \frac{\mu_{iK} \omega_{iK}}{\hbar} (\delta_{x,u-1} - \delta_{x,u+1}) \langle x | Q_K | u \rangle \\ &= - \langle u | \frac{\partial}{\partial Q_K} | x \rangle = \frac{-\mu_{jK} \omega_{jK}}{\hbar} (\delta_{u,x-1} - \delta_{u,x+1}) \langle u | Q_K | x \rangle, \end{aligned} \quad (15)$$

where ω_{iK} is the angular frequency of the K^{th} mode for the i^{th} electronic level, we are now in a position to write down the scattering tensor to first order in h_{ij}^K . Due to the large energy denominator, the first term in (1) can be neglected for resonance excitation and the sum over states in the last term can be restricted to those states $|iu\rangle$ such that $E_{iu} - E_{gw} \approx hv$, where $E_{gw} = E_{g0} + \epsilon_w$, E_{g0} being the energy of the lowest vibrational level of the electronic ground state $|g\rangle$, and ϵ_w the vibrational energy of the w^{th} level. With these simplifications the scattering tensor at resonance can be written as,

$$(\alpha_{\rho\sigma})_{vw} = A_{\rho\sigma} + B_{\rho\sigma} + C_{\rho\sigma} + D_{\rho\sigma} + F_{\rho\sigma} \quad (16)$$

$$A_{\rho\sigma} = \sum_i \sum_u \frac{M_{ig}^{\rho} M_{gi}^{\sigma} \langle v | u \rangle \langle u | w \rangle}{E_{iu} - E_{gv_L} - hv - i\Gamma_{iu}} \quad (17)$$

$$B_{\rho\sigma} = \sum_i \sum_u \sum_{j \neq i} \sum_K \frac{h_{ij}^K}{(E_i^0 - E_j^0) (E_{iu} - E_{gv_L} - hv - i\Gamma_{iu})} \quad (18)$$

$$x \left\{ M_{ig}^{\sigma} M_{gj}^{\rho} \langle v|u \rangle \langle u|Q_K|w \rangle + M_{ig}^{\rho} M_{jg}^{\sigma} \langle v|Q_K|u \rangle \langle u|w \rangle \right\}$$

$$C_{\rho\sigma} = - \sum_i \sum_u \sum_{j \neq g} \sum_K h_{gj}^K \frac{M_{ji}^{\sigma} M_{ig}^{\rho} \langle v|Q_K|u \rangle \langle u|w \rangle + M_{gi}^{\sigma} M_{ig}^{\rho} \langle v|u \rangle \langle u|Q_K|w \rangle}{(E_{iu} - E_{gw} - \hbar\nu - i\Gamma_{iu})(E_j^0 - E_g^0)} \quad (19)$$

$$D_{\rho\sigma} = \sum_i \sum_u \sum_{j \neq i} \sum_x \sum_K \frac{h_{ij}^K}{(E_i^0 - E_j^0)(E_{iu} - E_{gv} - \hbar\nu - i\Gamma_{iu})} \quad (20)$$

$$x \left\{ \frac{\hbar\nu M_{Kig}^j M_{gj}^{\sigma} \langle v|\bar{u} \rangle \langle u|Q_K|x \rangle \langle x|w \rangle (\delta_{u,x-1} - \delta_{u,x+1})(E_{iu} - E_{jx})^{-1}}{K} \right\}$$

$$= \frac{\hbar\nu M_{Kig}^j M_{gj}^{\sigma} \langle v|x \rangle \langle x|Q_K|u \rangle \langle u|w \rangle (\delta_{x,u-1} - \delta_{x,u+1})(E_{iu} - E_{jx})^{-1}}{K}$$

$$F_{\rho\sigma} = - \sum_i \sum_u \sum_{j \neq g} \sum_x \sum_K \frac{h_{gj}^K}{(E_j^0 - E_g^0)(E_{iu} - E_{gw} - \hbar\nu - i\Gamma_{iu})} \quad (21)$$

$$x \left\{ \frac{M_{ji}^{\sigma} M_{ig}^{\rho} \hbar\omega_{jK} \langle v|Q_K|x \rangle \langle x|u \rangle \langle u|w \rangle (\delta_{v,x-1} - \delta_{v,x+1})(E_{gv} - E_{jx})^{-1}}{jK} \right\}$$

$$- \frac{M_{gi}^{\sigma} M_{ij}^{\rho} \hbar\omega_{gK} \langle v|u \rangle \langle u|x \rangle \langle x|Q_K|w \rangle (\delta_{x,w-1} - \delta_{x,w+1})(E_{gw} - E_{jx})^{-1}}{giK}$$

where $M_{ij}^{\rho} \equiv \langle 0|R_{\rho}|j_0 \rangle$. The physical interpretation of the terms of (16) will become clear when (16) is applied to Raman scattering in metalloporphyrins. The terms A, B, and C of (16) correspond to the A, B, and C

terms of Albrecht;¹⁷ however, the D and F terms, which result from the first order nonadiabatic correction, do not appear in the earlier theory.

As has been pointed out,³⁴ the conventional method of evaluating $\langle i | \frac{\partial}{\partial Q_K} | j \rangle$ employed in (11)-(14) must be used with caution. The energy denominator in (14) has been used by others to drastically reduce the number of intermediate states contributing to the Raman scattering through vibronic mixing, although in some cases systematic cancellation for nearby states may make coupling with states far away in energy non-negligible. However, the method appears safe for metalloporphyrin systems and has been retained here.

Another point that might be raised is whether terms with diagonal matrix elements of the form $\langle i | \frac{\partial}{\partial Q_K} | i \rangle$ are present, since they are omitted in the sum appearing in the conventional expansion (12), but are not formally excluded in the forms (9) and (10), for example. However, if the conventional expansion (i.e. (12)) is appropriate, then diagonal terms do not appear until second order in h_{ij}^K , e.g. in the term $\langle i | \frac{\partial^2}{\partial Q_K^2} | i \rangle$ in (8). This differs from the recently³⁵ modified theory of Peticolas³⁶ in which diagonal coupling matrix elements appear at first order.

The expression (16) with non-adiabatic coupling terms present (at least to first order) represents an improvement in the Albrecht theory--one which is essential in understanding the frequency dependence of Raman line intensities for Mn(III) porphyrins.

Structure and Symmetry of Metalloporphyrins

Metalloporphyrins³⁷ are metal ion containing macrocyclic tetrapyrrole structures which are formally derived from porphyrin by substi-

tution of some of the eight peripheral hydrogen atoms with various side groups and the two imino hydrogens with the centrally located metal ion. In metal etioporphyrin I (Figure 3) the 1, 3, 5, and 7 positions carry methyl side chains, the 2, 4, 6, 8 positions carry ethyl side chains. In manganese(III) etioporphyrin I complexes the Mn(III) ion requires an additional negative valence ligand. These anions were chloride, iodide, and thiocyanate radicals in the present study.

The symmetry of Mn(III)EtioIX is formally C_4 , however, the porphyrin skeleton itself permits use of D_{4h} symmetry classification. For comparison with other metalloporphyrin studies it is convenient to use the higher symmetry labels, although normal modes containing contributions from the peripheral substituents will reflect lower symmetry.

Metalloporphyrin Excited States

In this section we outline the pertinent features of low lying excited states for metalloporphyrins having typical absorption spectra. A four orbital model⁴ has been proposed by Gouterman on the basis of molecular orbital calculations. The model is supported by optical absorption, emission, and magnetic circular dichroism (MCD) spectra and the effects on the first two due to changes in the substituents.^{3,38}

Molecular orbital calculations^{4,39} indicate the highest filled molecular orbitals of the π -ring system to be non-degenerate orbitals of symmetry $a_{1u}(\pi)$ and $a_{2u}(\pi)$. The lowest unfilled orbitals are doubly-degenerate orbitals of $e_g(\pi^*)$ symmetry. The ground state configuration ($a_{1u}^2(\pi), a_{2u}^2(\pi)$) gives rise to a molecular ground state of A_{1g} symmetry; the two singly excited configurations ($a_{1u}(\pi), e_g(\pi^*)$) and ($a_{2u}(\pi),$

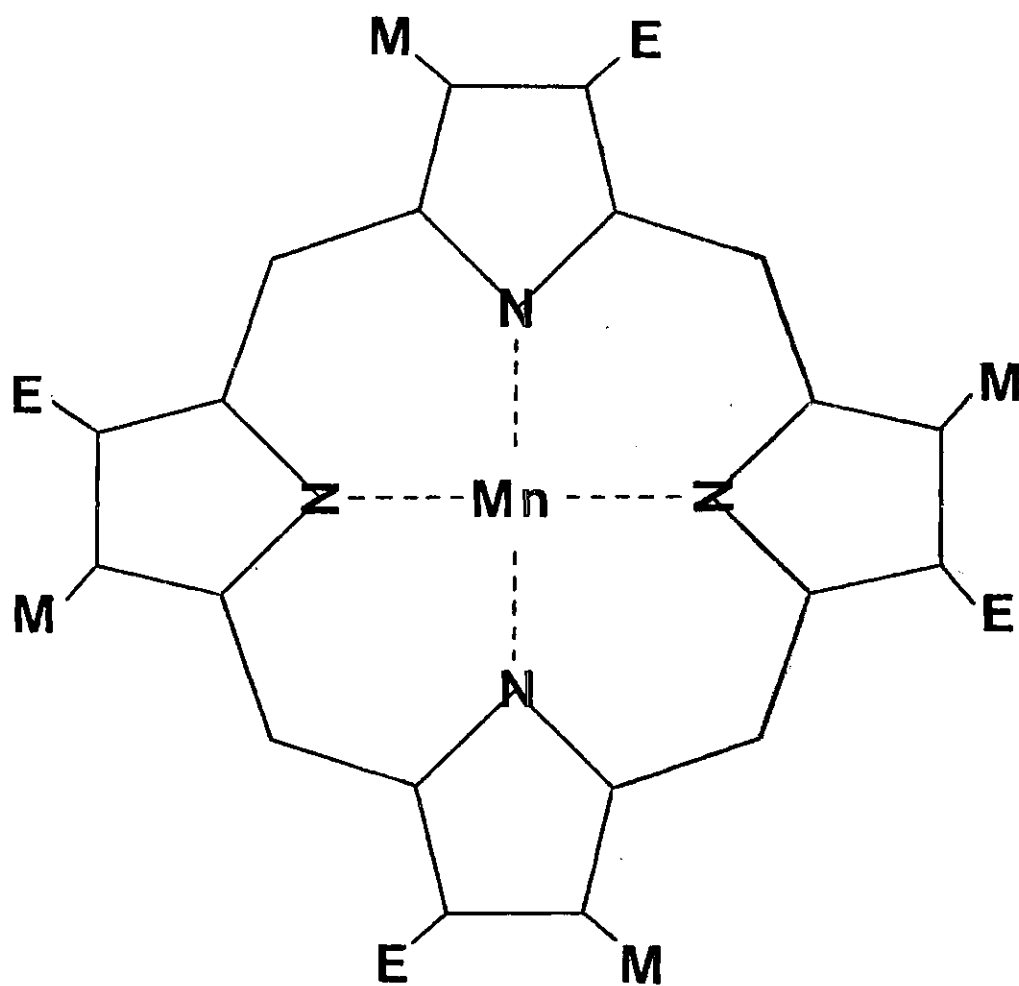


Figure 3. Structure of Manganese(III) Etioporphyrin I: The Anion is Complexed to the Metal Above the Plane. (M=Methyl, E=Ethyl)

$e_g(\pi^*)$ give rise to doubly-degenerate molecular states of E_u symmetry. (Figure 4) In all molecular orbital calculations the $a_{2u}(\pi)$ orbital lies much higher than the $a_{1u}(\pi)$ orbital. However, due to the crudeness of the calculations it is expected that the top filled orbitals are actually much closer in energy. Thus, it is expected that the two excited E_u molecular states are nearly degenerate (accidental), and, consequently, they are strongly mixed via the interaction between the electrons in the two configurations. The E_u molecular states, Q and B (Figure 4), arising from the perturbation yield sharply different transition moments; the state B gaining most of the intensity, while intensity in the Q band absorption occurs primarily by vibronic coupling³³ to the B band(Soret).⁴⁰ (Figure 1)

Vibronic Coupling in Metalloporphyrins

In order to introduce the ideas of vibrational coupling, we briefly consider vibronic borrowing of intensity³³ in the absorption spectrum of metalloporphyrins. Using arguments similar to those employed in deriving the scattering tensor (16), the transition dipole for absorption from the lowest vibrational level of the ground state to an excited state vibrational level can be shown to be,

$$\langle iu | R_\rho | g0 \rangle = M_{ig} \langle u | 0 \rangle + \sum_j \sum_K \frac{M_{ig}^\rho h_{ji}^K \langle u | Q_K | 0 \rangle}{E_i^0 - E_j^0}, \quad (22)$$

where the symbols are defined as before, and the non-adiabatic contribution has been omitted.³⁴ The contribution to the absorption (or extinction coefficient, ϵ) from the transition $|g0\rangle \rightarrow |iu\rangle$ is proportional to

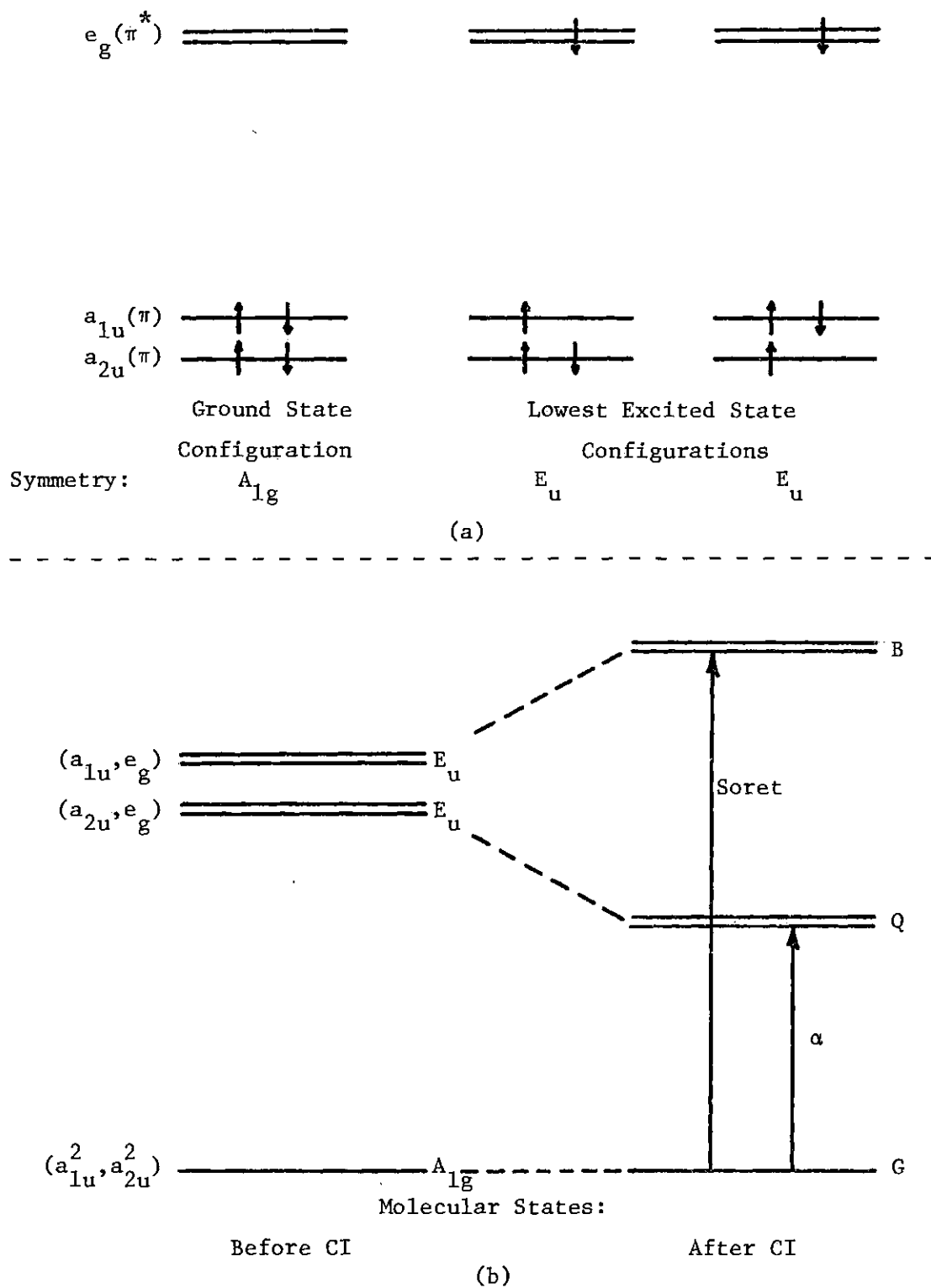


Figure 4. Ground and Excited State (a) Configurations and (b) Molecular States Before and After Configuration Interaction

$$|\langle iu | R_\rho | g0 \rangle|^2$$

For the state Q the transition dipole M_{QG}^{ρ} is small, therefore, the first term in (22) is negligible for the $|G0_L\rangle \rightarrow |Q1_L\rangle$ transition. Here $|G0_L\rangle \rightarrow |Q1_L\rangle$ indicates the transition from the electronic ground state with no vibrational modes excited to the excited state Q where the L^{th} mode is excited by one quantum; the occupation number of the other mode is zero. In the second term, the energy denominator and M_{jG}^{ρ} favor nearby states j which are strongly allowed. For metalloporphyrins all states in the sum over state in (22), except B, can be neglected due to (1) the larger energy denominator and (2) the usually small (compared to B) electronic transition dipole for other allowed $\pi \rightarrow \pi^*$ states. (The possible symmetry types for $\pi \rightarrow \pi^*$ orbitals-- a_{1u} , a_{2u} , b_{1u} , b_{2u} , and e_g , are determined by the antisymmetry of π orbitals with respect to reflection in the X-Y plane of the molecule. Thus, the possible molecular states arising from singly-excited configurations are of A_{1g} , A_{2g} , B_{1g} , B_{2g} , and E_u symmetry, and of these only the E_u states are electric dipole allowed.) In addition, metalloporphyrins have no permanent dipole moment, and M_{GG}^{ρ} , $\rho = X, Y, Z$ vanishes. As a consequence the transition dipole for the 0-1 transition for the state Q and the L^{th} vibrational (i.e. $G0_L \rightarrow Q1_L$) mode is,

$$\langle Q1 | R_\rho | G0 \rangle \approx M_{BG}^{\rho} h_{BQ}^L \langle 1 | Q_L | 0 \rangle [E_B^0 - E_Q^0]^{-1} \quad (23)$$

where we have assumed $|\langle 1 | Q_K | 0 \rangle| \ll |\langle 1 | Q_L | 0 \rangle|$, ($L \neq K$), in keeping only the L^{th} term in the sum over normal modes. (See below.)

Two predictions result from (23): (1) a vibrationally induced (0-1) absorption band should appear on the high energy side of the $G_0 \rightarrow Q_0$ (0-0) transition (Figure 1) and (2) a large contribution to the absorption in the Q band should come from those vibrations effective in coupling Q and B through h_{BQ}^K . The 0-0 absorption peak is called the α band and the 0-1 peak the β band.

The symmetry of the vibrations effective in coupling Q and B can be determined from the matrix elements h_{BQ}^K defined by (13). The operator $\left(\frac{\partial V}{\partial Q_K}\right)_{Q=0}$ has the same symmetry in the space of the electrons that Q_K has in the configuration-space of the nuclei.¹⁶ For h_{BQ}^K not to vanish, the direct product of the irreducible representations to which the states B and Q belong must contain the irreducible representation of the K^{th} normal mode.⁴¹ Since both B and Q are E_u states, reference to a character table for the group D_{4h} gives,

$$\Gamma_B \times \Gamma_Q = \Gamma_{E_u} \times \Gamma_{E_u} = a_{1g} + a_{2g} + b_{1g} + b_{2g}, \quad (24)$$

that is, only vibrational modes of a_{1g} , a_{2g} , b_{1g} , and b_{2g} symmetries can couple the states Q and B. Thus, modes of these symmetries contribute to the 0-1 absorption band for the Q state. Furthermore, since the matrix element, h_{QB}^K , appears in the resonance Raman scattering tensor (16), this selection rule also determines which vibrational modes will contribute to the Raman scattering for all of the terms of (16) other than the A term. In the cyclic polyene model of Perrin, Gouterman, and Perrin,⁴⁰ only the non-totally symmetric vibrations of a_{2g} , b_{1g} , and b_{2g} symmetry are vibronically active. Although allowed group-theoretically, the a_{1g}

vibration is inactive in this model which also discards bending modes. Consideration of porphyrin rather than a sixteen membered cyclic polyene, shows that it is feasible for pyrrole ring coordinates of a_{1g} symmetry to be vibronically active also. (Chapter V).

Resonance Raman Scattering in Metalloporphyrins

It has been demonstrated⁴² experimentally that vibrations effective in mixing Q and B states dominate the Raman spectrum in metalloporphyrins and in related heme proteins for resonance excitation in the Q band. On the other hand, it is the totally symmetric modes which dominate the Raman spectrum upon excitation into the B (Soret) band.⁴³ In this section these general features of resonance Raman scattering in metalloporphyrins are examined in terms of the scattering tensor (16). The polarization properties of the Raman active modes are also considered.

Some simplification of the scattering tensor (16) is possible for metalloporphyrin systems. First, the Q and B bands are each composed of two degenerate states, Q_X, Q_Y , and B_X, B_Y , which form the basis for an E_u representation of the D_{4h} group. The components of the states Q and B can be labeled X and Y, since the pair of coordinates X, Y transform like E_u . As a consequence, the sum over the resonant states i in (17)-(21) includes $i = Q_X, Q_Y$ for excitation into the Q band, and includes $i = B_X, B_Y$ for resonance with the Soret.

Second, as in the previous section the lack of a permanent electric dipole moment and the large energy denominator $E_j^0 - E_G^0$ allows us to neglect the terms C and F of (16) involving vibronic coupling with the ground state. Third, the energy denominator $E_i^0 - E_j^0$ in the B and D terms

suggests that only nearby, strongly-allowed states need be considered in the sum over states j . For example, since the B state is typically near the state $Q(E_B^0 - E_Q^0 \geq 5000 \text{ cm}^{-1})$ and strongly allowed, the terms with $j = B_X, B_Y$ dominate the sum over j for resonance with the Q band. Finally, the D term can probably be neglected, since an extra factor of $h\omega_K/5000 \text{ cm}^{-1} < 1/3$ appears in the D term but not in the B term.

With these simplifications the Raman scattering tensor for the fundamental of the L^{th} normal mode can be written as,

$$(\alpha_{\rho\sigma})_{0 \rightarrow 1_L} \approx A_{\rho\sigma}^{0 \rightarrow 1_L} + B_{\rho\sigma}^{0 \rightarrow 1_L} \quad (25)$$

where for resonance with the Q band,

$$A_{\rho\sigma}^{0 \rightarrow 1_L} = \sum_{Q=Q_X, Q_Y} \sum_u \frac{M_{QG}^{\rho} M_{GQ}^{\sigma} \langle 1|u\rangle \langle u|0\rangle}{E_{Qu} - E_{G0} - h\nu - i\Gamma_{Qu}} \quad (26)$$

$$B_{\rho\sigma} = - \sum_{Q=Q_X, Q_Y} \sum_u \sum_{B=B_X, B_Y} \sum_K \frac{h_{QB}^K}{(E_B^0 - E_Q^0)(E_{Qu} - E_{G0} - h\nu - i\Gamma_{Qu})} \quad (27)$$

$$\times \left\{ M_{QG}^{\sigma} M_{GB}^{\rho} \langle 1|u\rangle \langle u|Q_K|0\rangle + M_{QG}^{\rho} M_{GB}^{\sigma} \langle 1|Q_K|u\rangle \langle u|0\rangle \right\}$$

and similar expressions hold for excitation into the B band. In (25)-(27), the zero temperature approximation ($|w\rangle = |0\rangle$, $|v\rangle = |1_L\rangle$) has been made, and is appropriate since the frequency of the vibrations of interest are

greater than the thermal frequency, $kT = 200 \text{ cm}^{-1}$.

The qualitative features of Q band resonance Raman spectra can now be explained in terms of the relative contribution to Raman scattering from the A and B terms (26) and (27). Ignoring the Frank-Condon factors for the moment, we see that the A term is proportional to M_{QG}^2 , whereas the B term is proportional to $h_{GB}^K M_{QG} M_{BG} [E_B^0 - E_Q^0]^{-1}$. Since $M_{QG} < M_{BG}$, it is conceivable that the extra energy denominator of the B term (typically, $E_B^0 - E_Q^0 = 6000 \text{ cm}^{-1}$) can be compensated by the presence of the larger transition dipole of the B state, provided the vibronic coupling energy, h_{QB}^K , is sufficient. This is actually the case for metalloporphyrins when excitation is in the Q band absorption. As a consequence, the B term of (25) dominates, and primarily non-totally symmetric vibrations which couple B and Q dominate the Raman spectra. This view is substantiated by estimates⁴⁴ of the vibronic coupling energy (4000 cm^{-1}) in the related cobalamin complexes placing it close to the energy gap between Q and B.

In contrast, upon excitation into the Soret band, it is the A term contribution which is enhanced, since now the A term is quadratic in the stronger transition dipole of the Soret band. For there to be an A term contribution at all, the potential curve of the ground state must differ from the excited state potential curve, otherwise $\langle 1 | u \rangle \langle u | 0 \rangle = 0$ for all u due to orthogonality of the harmonic oscillator wavefunctions of the ground and excited states.⁴⁵ Usually, the molecular distortion in the excited state is totally symmetric and, as such can be resolved into components along only the totally symmetric normal modes; hence, only totally symmetric modes can gain intensity from the A terms. Indeed,

it is the a_{1g} modes which dominate the Raman spectrum for Soret band resonance excitation.

We now turn to the polarization properties of the Raman active modes. The symmetry of the vibrations appearing in the Raman spectrum is obtained from these polarization properties of the Raman lines. The depolarization ratio ρ is defined by

$$\rho = \frac{I_{\perp}}{I_{\parallel}} \quad (28)$$

where I_{\perp} and I_{\parallel} are the scattered intensities polarized perpendicular and parallel to the polarization of the incident light. From tabulated⁴⁶ tensor patterns for D_{4h} symmetry (or directly from (25) and Table I), the predicted depolarization ratio for a mode of a given symmetry in terms of the tensor invariants δ_F , δ_G , and δ_H is,

$$\rho = \frac{-\delta_F + 4\delta_G - \delta_H}{2(\delta_F + \delta_G + \delta_H)} \quad (29)$$

where the tensor invariants are defined by

$$\delta_F = \sum_{\rho, \sigma} (\alpha_{\rho\rho})(\alpha_{\sigma\sigma})^* \quad (30)$$

$$\delta_G = \sum_{\rho, \sigma} (\alpha_{\rho\sigma})(\alpha_{\rho\sigma})^* \quad (31)$$

and

$$\delta_H = \sum_{\rho, \sigma} (\alpha_{\rho\sigma})(\alpha_{\sigma\rho})^* \quad (32)$$

The tensor patterns for the Raman active modes (D_{4h} symmetry) are:

$$(\alpha_{\rho\sigma})_{a_{1g}} = \begin{bmatrix} S_1 & 0 & 0 \\ 0 & S_1 & 0 \\ 0 & 0 & S_2 \end{bmatrix} \quad (33)$$

$$(\alpha_{\rho\sigma})_{a_{2g}} = \begin{bmatrix} 0 & S_3 & 0 \\ -S_3 & 0 & 0 \\ 0 & 0 & 0 \end{bmatrix} \quad (34)$$

$$(\alpha_{\rho\sigma})_{b_{1g}} = \begin{bmatrix} S_4 & 0 & 0 \\ 0 & -S_4 & 0 \\ 0 & 0 & 0 \end{bmatrix} \quad (35)$$

$$(\alpha_{\rho\sigma})_{b_{2g}} = \begin{bmatrix} 0 & S_5 & 0 \\ S_5 & 0 & 0 \\ 0 & 0 & 0 \end{bmatrix} \quad (36)$$

From the tensor patterns (33)-(36), the invariants δ_F , δ_G , and δ_H are obtained from (30)-(32) for each symmetry, and (29) gives the depolarization ratio. The results are: $\rho_{a_{1g}} = 1/8$, $\rho_{a_{2g}} = \infty$, $\rho_{b_{1g}} = \rho_{b_{2g}} = 3/4$.

The a_{1g} vibrations are polarized (p); the a_{2g} vibrations are inversely (or anomalously) polarized (ip or ap); and the b_{1g} and b_{2g} vibrations are depolarized (dp).

Examination of the character table for the group D_{4h} shows that the tensor components α_{XZ} and α_{YZ} belong to the e_g representation;

therefore, modes of this symmetry may be Raman active, in addition to the a_{1g} , a_{2g} , b_{1g} , and b_{2g} modes which couple E_u states. Modes of e_g symmetry derive intensity by coupling an E_u state with states of A_{1g} , A_{2g} , B_{1g} , or B_{2g} symmetry. For metalloporphyrins, states of the required symmetry are not sufficiently near the Q and B states, for Raman scattering from coupling with these states to be of the same magnitude as scattering due to Q-B coupling. For e_g vibrational modes the depolarization ratio varies between 3/4 away from resonance to a possible resonance value of 2.

Frequency Dependence of Raman Intensities
in Metalloporphyrins

Before examining resonance Raman scattering in atypical metalloporphyrins such as Mn(III) porphyrins, and, in particular, the dependence of Raman intensities on the frequency of the exciting radiation, it is of interest to see how the Raman frequency dependence is obtained from (25) for typical metalloporphyrins.⁴⁷ For excitation in the Q band region, (25) holds with A and B terms given by (26) and (27). First, consider a vibration which drives its intensity from the B term. These vibrations, called Herzberg-Teller modes, are primarily the non-totally symmetric modes. The frequency dependence is contained in the energy denominators of the terms in the sums indicated in (27). In principle the frequency dependence may be quite complicated. Fortunately, the Frank-Condon factors and transition moments in the numerator determine which terms in the sum over u and K will be most significant. Assuming the potential curves for the L^{th} normal mode in the ground state and the state Q are identical, all terms in the sum over K vanish except

for $u = 0, 1$ due to orthogonality of the harmonic oscillator wavefunctions.

In this case (27) reduces to

$$B_{\rho\sigma} = - \sum_{Q=Q_X, Q_Y} \sum_{B=B_X, B_Y} \frac{h_{QB}^L}{E_B^0 - E_Q^0} \left\{ \frac{M_{QG}^\sigma M_{GB}^\sigma}{E_{Q1}^0 - E_{G0}^0 - \hbar\nu - i\Gamma_{Q1}} \right. \quad (37)$$

$$\left. + \frac{M_{QG}^\sigma M_{GB}^\sigma}{E_{Q0}^0 - E_{G0}^0 - \hbar\nu - i\Gamma_{Q0}} \right\}$$

Given the symmetry of the vibration further simplification⁴⁷ is possible. In the next section, the symmetry required for a normal mode to couple Q_X , Q_Y , B_X , and B_Y by one-electron operators, such as h^L , are determined, and displayed in Table I in terms of the one-electron matrix elements. For example, from Table I, $h_{Q_X B_Y}^L = -h_{Q_Y B_X}^L$, and $h_{QB}^L = 0$ otherwise, for an a_{2g} vibration. In addition, transition moments like $M_{Q_X G}^Y \equiv \langle Q_X | R_Y | G \rangle_0 = 0$, since $R_Y | G \rangle_0$ and $Q_X | G \rangle_0$ transform like different rows of the same unitary representation.⁴¹

With these additional simplifications the XY tensor component for an a_{2g} mode becomes,

$$B_{XY}^L = - \frac{h_{Q_X B_Y}^L M_{QG}^\sigma M_{GB}^\sigma}{E_B^0 - E_Q^0} \left\{ \frac{1}{E_{Q0}^0 - E_{G0}^0 - \hbar\nu - i\Gamma_{Q0}} - \frac{1}{E_{Q1}^0 - E_{G0}^0 - \hbar\nu - i\Gamma_{Q1}} \right\} \quad (38)$$

Also, note that $B_{YX}^L = -B_{XY}^L$ and $B_{\rho\sigma}^L = 0$, $\rho \sigma \neq X, Y$, (i.e. the scattering tensor is antisymmetric for an a_{2g} mode as in (34)).

For the a_{1g} , b_{1g} , and b_{2g} vibrations a similar expression holds,

except a + sign occurs between the two terms in (38). From the Appendix, equation (A-17), the intensity I_B for a Herzberg-Teller mode is proportional to $\sum_{\rho, \sigma} |B_{\rho\sigma}^L|^2$. Figure 5 shows a plot of

$$I_B \propto \left| \frac{1}{E_{Q0} - E_{G0} - h\nu - i\Gamma_{Q0}} \pm \frac{1}{E_{Q1} - E_{G0} - h\nu - i\Gamma_{Q1}} \right|^2 \quad (39)$$

where the upper (lower) sign holds for a_{1g} , b_{1g} , and b_{2g} (a_{2g}) modes. The minus (plus) sign results in more (less) intensity between the 0-0 and 0-1 maxima and shifts these peaks toward (away from) each other. Note that the 0-0 and 0-1 intensities are equal.

In arriving at these results we have assumed the potential curves in the states G and Q are identical. This assumption is supported by the near equality of the vibrational frequencies for the ground state and the state Q.⁴⁸ Furthermore, only a very small shift in the equilibrium position is expected for non-totally symmetric modes.⁴⁴

For modes which derive intensity from the A term, called Frank-Condon modes, the Frank-Condon factors again determine which of the terms in the sum over u are significant.⁴⁷ Primarily a_{1g} modes acquire intensity from the A term, since it is usually along these modes that the molecule is distorted in the excited state. The frequencies of the Raman active a_{1g} vibrations in the ground state and the state Q are nearly equal; however, a small shift in the equilibrium position of the potential curves is expected. In a study of the cobalamin complexes⁴⁴ the shift, Δ , for the 1502 cm^{-1} Raman mode was found to be 0.35 in dimensionless coordinates $\xi_K \equiv \sqrt{\frac{m_K \omega_K}{2h}} Q_K$, where ω_K is the angular frequency in both the ground state and the excited state and m_K is the mass associated

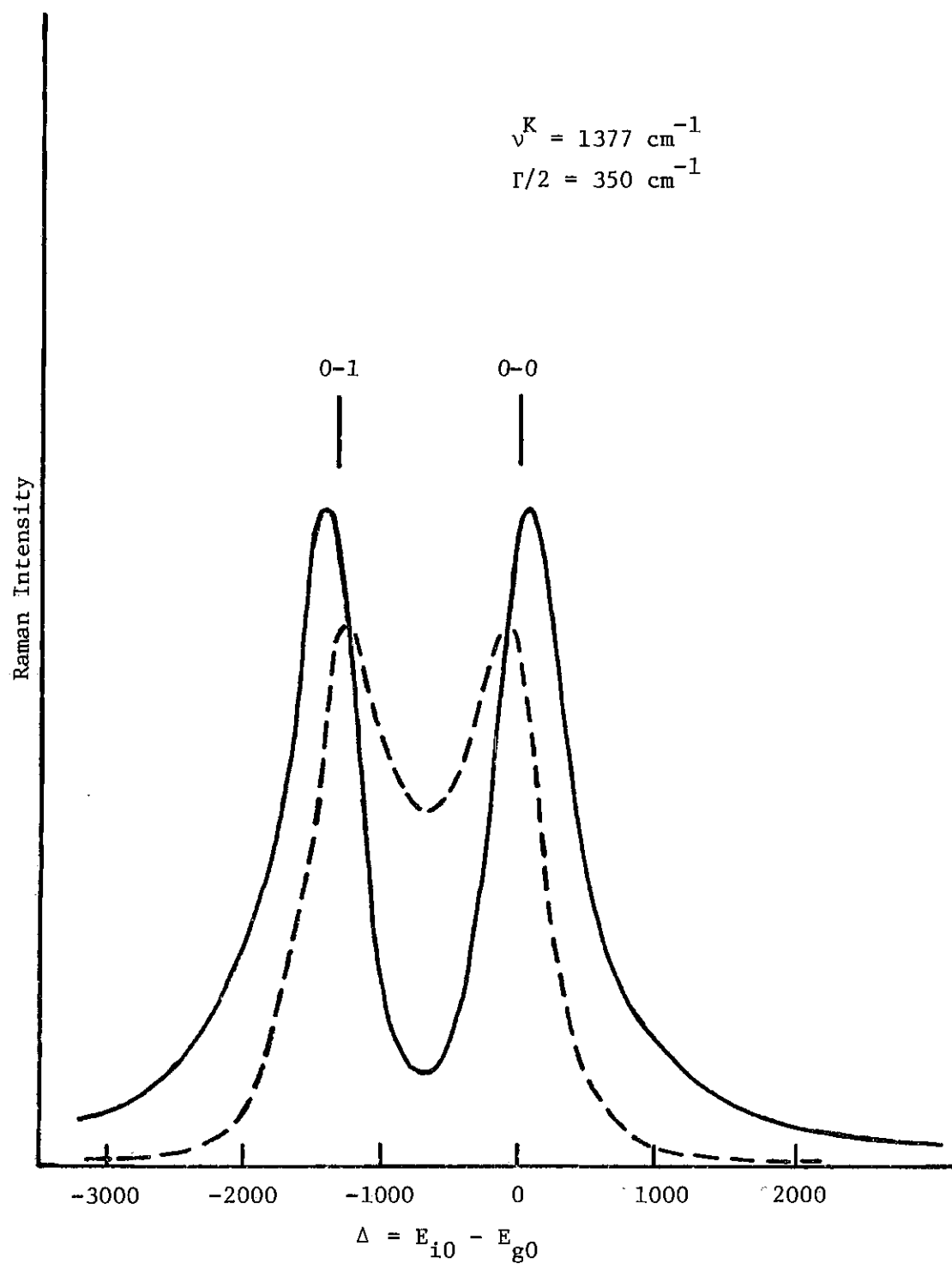


Figure 5. Raman Intensity as a Function of Exciting Frequency:
 B Term Only, - - - - Minus Sign (a_{2g} , a_{1g} —Frank-Condon),
 ————— Plus Sign (b_{1g} , b_{2g} , a_{1g} —Herzberg-Teller)

with the K^{th} normal mode. In these coordinates the root mean square displacement, $(\langle \xi_K^2 \rangle)^{1/2}$, for the lowest vibrational level is equal to one.

In order to determine which of the terms in the sum over vibrational levels is largest in (17), the Frank-Condon factors are calculated assuming a shift, Δ_K , in the equilibrium position, and assuming the vibrational frequency in the ground and excited states is the same. Under these assumptions the harmonic oscillator wave functions are:

$$(\xi_K | v_K) = N_{v_K} H_{v_K}(\xi_K) e^{-\xi_K^2/2} \quad (40)$$

for the ground state, and in the excited state,

$$(\xi_K | u_K) = N_{u_K} H_{u_K}(\xi_K - \Delta_K) e^{-(\xi_K - \Delta_K)^2/2} \quad (41)$$

where $H_{u_K}(\xi_K)$ is the u_K^{th} Hermite polynomial and N_{u_K} is the normalization constant $\sqrt{\pi} 2^{u_K/2} u_K!$.

The overlap factor $(u_K | v_K)$ for the K^{th} normal mode is calculated⁴⁹ from (40) and (41),

$$(u_K | v_K) = (u_K! v_K!)^{-1/2} e^{-\Delta_K^2/2} \sum_m^{\min(u_K, v_K)} \frac{(-1)^{v_K-m} u_K! v_K! \Delta_K^{u_K+v_K-2m}}{(u_K-m)! m! (v_K-m)!} \quad (42)$$

which for $v_K = 0$, becomes,

$$Q(u_K | 0)_G = (u_K!)^{-1/2} \Delta_K^{u_K} e^{-\Delta_K^2/2} \quad (43)$$

and for $v_K = 1$,

$$Q(u_K | 1)_G = (u_K!)^{-1/2} e^{-1/2 \Delta_K^2} \begin{bmatrix} u_K^{-1} & u_K+1 \\ u_K \Delta_K & -\Delta_K \end{bmatrix} \quad (44)$$

From (43) and (44) it is clear that the overlap factors go rapidly to zero as u_K increases if the shift Δ_K is less than unity. For example, if $\Delta = 0.5$, the ratio of $(2|0)$ to $(0|0)$ is already 0.18.

The Frank-Condon factors appearing in (17) or (26) can be written in terms of (43) and (44) as,

$$\langle 1|u \rangle \langle u|0 \rangle = (1|u_L)(u_L|0) \prod_{K \neq L} (0|u_K)(u_K|0) = (1|u_L)(u_L|0) F_L \quad (45)$$

From (45) it is observed that the largest terms are those for which a maximum number of the overlap factors $(u_K|v_K)$ appear with $u_K = v_K$. Two terms will be large--the terms with $u_L = 0$ and 1, with $u_K = 0$ for $K \neq L$. Neglecting all but these two terms, the intensity from the A term is proportional to

$$\begin{aligned} I_A & \sim \left| \frac{G(1|1)_{QQ}(1|0)_G}{E_{Q1} - E_{G0} - \hbar\nu - i\Gamma_{Q1}} + \frac{G(1|0)_{QQ}(0|0)_G}{E_{Q0} - E_{G0} - \hbar\nu - i\Gamma_{Q0}} \right|^2 \quad (46) \\ & = Q(1|0)_G \left| \frac{G(1|1)_Q}{E_{Q1} - E_{G0} - \hbar\nu - i\Gamma_{Q1}} - \frac{Q(0|0)_G}{E_{Q0} - E_{G0} - \hbar\nu - i\Gamma_{Q0}} \right|^2 \\ & = \Delta e^{-\Delta^2} \left| \frac{1 - \Delta^2}{E_{Q1} - E_{G0} - \hbar\nu - i\Gamma_{Q1}} - \frac{1}{E_{Q0} - E_{G0} - \hbar\nu - i\Gamma_{Q1}} \right|^2 \end{aligned}$$

For $\Delta < 1$, the frequency dependence for a Frank-Condon mode from (46)

is similar to that for an a_{2g} mode (see Figure 5), since the sign between terms is minus. However, the intensity at the 0-1 peak must be less than at the 0-0 peak since the numerators are unequal in this case, and the ratio of the 0-0 and 0-1 intensities may provide an estimate of the shifts in the potential curves.

Inclusion of Charge Transfer States

For the atypical metalloporphyrins, e.g. Cr(III), Fe(III), and Mn(III) porphyrins, extra bands appear in the optical absorption spectrum, which are not attributable to the Q and B states of typical metalloporphyrins. These bands may arise from low lying transitions from porphyrin molecular orbitals to metal orbitals or from metal-to-porphyrin transitions, i.e. charge transfer transitions. In a recent study of the Cr(III), Mn(III), and Fe(III) hyperporphyrins Gouterman *et al.*¹¹ offered band assignments for the Cr(III) porphyrin absorption spectra. Arguments advanced there show that the iterative extended Huckel calculations considerably underestimate the energy of charge transfer transitions. If, contrary to the calculation for Cr(III) porphyrins, the charge transfer states ($a_{1u}(\pi)$, $a_{2u}(\pi) \rightarrow e_g(d_\pi)$) were higher in energy than the $\pi \rightarrow \pi^*$ states ($a_{1u}(\pi)$, $a_{2u}(\pi) \rightarrow e_g(\pi^*)$), then the authors obtained a consistent interpretation of Cr(III) porphyrin emission and absorption spectra. They proposed that Band V in the absorption spectra of Cr(III) complexes is mainly Soret-like, while the near uv bands contain appreciable $a_{2u}(\pi)$, $a_{1u}(\pi) \rightarrow e_g(d_\pi)$ charge transfer character. These arguments were extended to Mn(III) complexes, placing the energy of the porphyrin-to-metal d_π transition near that of the $\pi \rightarrow \pi^*$ state. Figure 6. It is

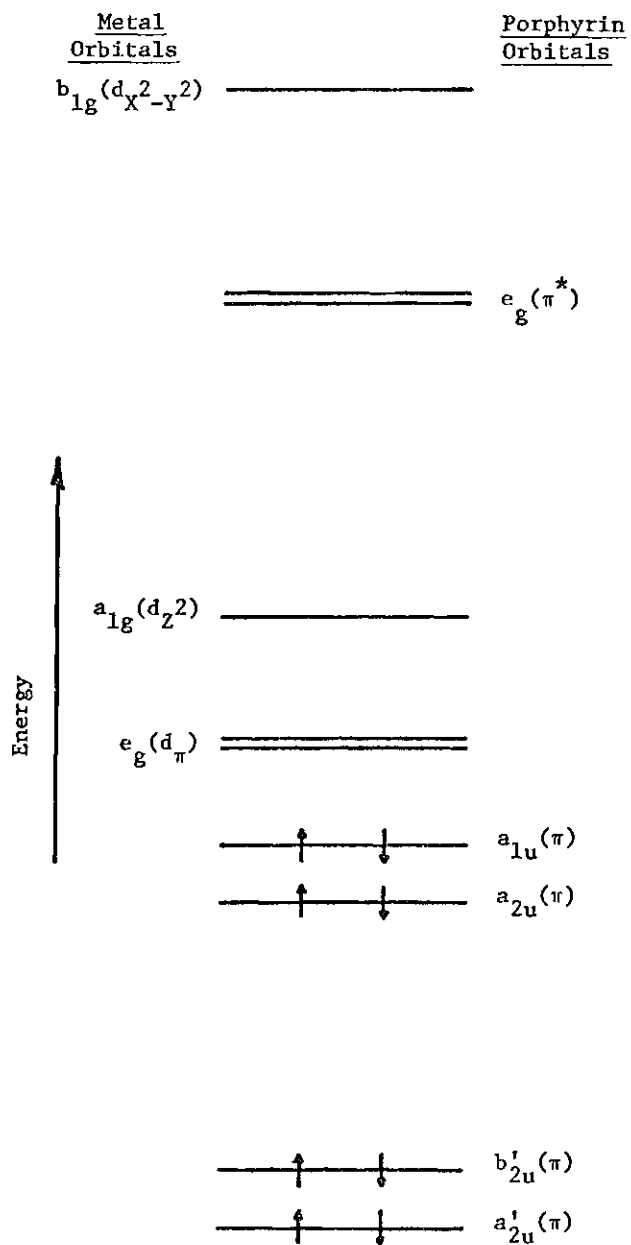


Figure 6. Manganese(III) Porphyrin Molecular Orbital Energy Levels⁸ for the Ground State Including Metal d-Orbitals

proposed that the four configurations of E_u symmetry arising from the promotions $a_{2u}(\pi), a_{1u}(\pi) \rightarrow e_g(\pi^*)$ and $a_{2u}(\pi), a_{1u}(\pi) \rightarrow e_g(d)$ suffer configuration interaction (CI) to yield the states evident in bands III, V, V_a , and VI of the Mn(III) porphyrin absorption spectrum (Figure 2). This "8-orbital model" is developed in this section and the qualitative features of resonance Raman scattering for such a system are discussed.

Boucher has proposed^{8,9} that some of Band III-VI and V_a correspond to the allowed out-of-plane charge transfer transition, $a'_{2u}(\pi) \rightarrow a_{1g}(d_{z^2})$, and the in-plane transitions, $b'_{2u}(\pi), a'_{2u}(\pi) \rightarrow e_g(d_{\pi})$, where the primed orbitals are the next-to-highest filled π -orbitals. If the in-plane charge transfer transitions proposed by Boucher mix with the $\pi \rightarrow \pi^*$ transitions, then the Raman scattering differs from the model proposed and discussed here in this section. In view of this difference the donor orbitals may be distinguishable by resonance Raman studies.

The resonance Raman scattering amplitudes for non-totally symmetric modes are determined by the vibrational coupling matrix elements

$\langle i | (\partial V_{Ne} / \partial Q_K)_0 | j \rangle$ where $|i\rangle$ and $|j\rangle$ are the CI mixed molecular states. We employ as basis for $|i\rangle$ a 50-50 mixture of singly excited configurations which represent Q and B states and use this ratio as well for charge transfer states C and D. The states $|i\rangle$ are multielectron Slater determinants of the spin molecular orbitals. However, in writing expressions for the states only the partially filled orbitals are shown explicitly; the X-components of the two $\pi \rightarrow \pi^*$ states are:³

$$|B_X^*\rangle \equiv (2)^{-1/2} [(a_{2u} e_{gX}) - (a_{1u} e_{gY})] \quad (47a)$$

$$|Q_X\rangle \equiv (2)^{-\frac{1}{2}}[(a_{2u}e_{gX}) + (a_{1u}e_{gY})] \quad (47b)$$

and, the X-components of the charge transfer states are:

$$|C_X\rangle \equiv (2)^{-\frac{1}{2}}[(a_{2u}d_{XZ}) - (a_{1u}d_{YZ})] \quad (48a)$$

$$|D_X\rangle \equiv (2)^{-\frac{1}{2}}[(a_{2u}d_{XZ}) - (a_{1u}d_{YZ})] \quad (48b)$$

For the Y-components of B and Q,

$$|B_Y\rangle \equiv (2)^{-\frac{1}{2}}[(a_{2u}e_{gY}) + (a_{1u}e_{gX})] \quad (49a)$$

$$|Q_Y\rangle \equiv (2)^{-\frac{1}{2}}[(a_{2u}e_{gY}) - (a_{1u}e_{gX})] \quad (49b)$$

and, the Y-components of the charge transfer states C and D are:

$$|C_Y\rangle \equiv (2)^{-\frac{1}{2}}[(a_{2u}d_{YZ}) + (a_{1u}d_{XZ})] \quad (50a)$$

$$|D_Y\rangle \equiv (2)^{-\frac{1}{2}}[(a_{2u}d_{YZ}) - (a_{1u}d_{XZ})] \quad (50b)$$

with $(a_{1u}d_{XZ}) \equiv (2)^{-\frac{1}{2}}(|\bar{a}_{1u}d_{XZ}| - |\bar{a}_{1u}d_{XZ}|)$ where the bar denotes a β spin-orbital in the determinant. Similar expressions hold for the other configurations.

Symmetries of one-electron operators which yield non-zero matrix elements are displayed in Table I. Perturbing operators which couple porphyrin π molecular orbitals are underlined, those that involve at least one metal-centered orbital (d_{XZ} , d_{YZ}) are not. The table is

Table 1. Symmetries Required to Mix States (Before CI) by One-Electron Perturbations*†

	B_X	B_Y	Q_X	Q_Y	C_X	C_Y	D_X	D_Y
B_X	$\underline{(-a_{1g} + a'_{1g})}$	0	$\underline{(-a'_{1g} + b_{1g})}$	$\underline{(a_{2g} + b_{2g})}$	$\underline{a'_{1g}}$	0	b_{1g}	b_{2g}
B_Y		$\underline{(-a_{1g} + a'_{1g})}$	$\underline{(-a_{2g} + b_{2g})}$	$\underline{(-a'_{1g} - b_{1g})}$	0	$\underline{a'_{1g}}$	b_{2g}	b_{1g}
Q_X			$\underline{(-a_{1g} + a'_{1g})}$	0	b_{1g}	b_{2g}	$\underline{a'_{1g}}$	0
Q_Y				$\underline{(-a_{1g} + a'_{1g})}$	b_{2g}	b_{1g}	0	$\underline{a'_{1g}}$
C_X	$\underline{a_{1g}} \equiv \frac{1}{2}[\langle a_{1u} h^K a_{1u} \rangle + \langle a_{2u} h^K a_{2u} \rangle]$ $\underline{a'_{1g}} \equiv \frac{1}{2}[\langle e_{gX} h^K e_{gX} \rangle + \langle e_{gY} h^K e_{gY} \rangle]$				$\underline{(-a_{1g} + a'_{1g})}$	0	$\underline{(-a'_{1g} + b_{1g})}$	$\underline{(a_{2g} + b_{2g})}$
C_Y	$\underline{a'_{1g}} \equiv \frac{1}{2}[\langle a_{2u} h^K a_{2u} \rangle - \langle a_{1u} h^K a_{1u} \rangle]$ $\underline{b_{1g}} \equiv \frac{1}{2}[\langle e_{gX} h^K e_{gX} \rangle - \langle e_{gY} h^K e_{gY} \rangle]$					$\underline{(-a_{1g} + a'_{1g})}$	$\underline{(-a_{2g} + b_{2g})}$	$\underline{(-a'_{1g} - b_{1g})}$
D_X	$\underline{b_{2g}} \equiv \langle e_{gX} h^K e_{gY} \rangle$						$\underline{(-a_{1g} + a'_{1g})}$	0
D_Y	$\underline{a_{2g}} \equiv \langle a_{1u} h^K a_{2u} \rangle$							$\underline{(-a_{1g} + a'_{1g})}$

* One-electron matrix element not involving metal orbitals are underlined.

† The table is symmetric.

obtained by forming the matrix elements of $\left(\frac{\partial V_{Ne}}{\partial Q_K}\right)_0$ with states from a row and column. For example, the Slater determinate representing the state $|B_Y\rangle$ is,

$$|B_Y\rangle = \frac{1}{2} \left\{ |a_1 \bar{a}_1 a_2 \bar{e}_Y| - |a_1 \bar{a}_1 \bar{a}_2 e_Y| + |a_2 \bar{a}_2 a_1 \bar{e}_X| - |a_2 \bar{a}_2 \bar{a}_1 e_X| \right\} \quad (51)$$

and, $|Q_X\rangle$ is given by,

$$|Q_X\rangle = \frac{1}{2} \left\{ |a_1 \bar{a}_1 a_2 e_X| - |a_1 \bar{a}_1 \bar{a}_2 e_X| + |a_2 \bar{a}_2 a_1 \bar{e}_Y| - |a_2 \bar{a}_2 \bar{a}_1 e_Y| \right\} \quad (52)$$

Substituting (51) and (52) into the matrix element

$\langle B_Y | \left(\frac{\partial V_{Ne}}{\partial Q_K}\right)_0 | Q_X \rangle$ gives,

$$\begin{aligned} \langle B_Y | \left(\frac{\partial V_{Ne}}{\partial Q_K}\right)_0 | Q_X \rangle &= \langle B | \sum_m h^K(m) | Q_X \rangle = \frac{1}{4} \left\{ 4 \langle e_{gY} | h^K | e_{gX} \rangle - 4 \langle a_{1u} | h^K | a_{2u} \rangle \right. \\ &\quad \left. + 4 \langle e_{gY} | h^K | e_{gX} \rangle - 4 \langle a_{1u} | h^K | a_{2u} \rangle \right\} \\ &= -\underline{a_{2g}} + \underline{b_{2g}} \end{aligned} \quad (53)$$

where orthogonality of the molecular orbitals has been used. In other matrix elements in the Table, one-electron matrix elements arising from other than the top-most four electrons cancel term-by-term. The expression for the diagonal elements in the table is obtained when the ground state perturbation energy is taken as zero. The last equality gives the symmetry of the modes which can give a non-vanishing one-electron

matrix element, and, hence, couple $|B_X\rangle$ and $|Q_X\rangle$: For instance, $|e_{gX}\rangle$ transforms like X; $|e_{gY}\rangle$ transforms like Y; therefore, a non-zero matrix element can result if the normal mode transforms like the product XY, which belongs to the b_{2g} representation.

Unless a vibration contains a significant contribution from a metal-nitrogen stretch, one-electron integrals of the form $\langle d_\pi | h_K | d_\pi \rangle$, $\langle d_\pi | h_K | a_{1u} \rangle$, or $\langle d_\pi | h_K | a_{2u} \rangle$ will be small compared to those involving porphyrin π orbitals alone, e. g. $\langle a_{1u} | h_K | a_{1u} \rangle$, etc. This arises (1) from the form of the one-electron coupling operator (Eq. 13), (2) from the localized character of the metal orbitals which results in diminished overlap between metal and porphyrin π orbitals, and (3) the small contribution from Mn-N stretching for Raman active modes. Zerner and Gouterman⁵⁰ have noted that d_π orbitals of transition metals will mix with porphyrin $e_g(\pi^*)$ orbitals; however, the acceptor molecular orbitals are 85-95% metal and are not significantly delocalized beyond the pyrrole nitrogens. Furthermore, preliminary calculations of Raman active modes⁵¹ and metal isotope shifts of infrared active vibrations (200-400 cm^{-1})⁵² suggest small (15%) contributions from $\nu(\text{Mn-N})$, even at low frequencies.

To see that one electron integrals involving the metal orbitals may indeed be small, consider, for example, the one-electron matrix element,¹⁶

$$\langle d_{XZ} | h^K | e_{gX} \rangle \equiv \int \chi_{d_{XZ}}^*(\vec{r}_i) \chi_{e_{gX}}(\vec{r}_i) h^K(\vec{r}_i) d\vec{r}_i \quad (54)$$

where

$$h^K(\vec{r}_i) = \sum_m \left[\frac{\partial \left(\frac{-eZ}{r_{im}} \right)}{\partial Q_K} \right]_0 = \sum_m \frac{-eZ_m (\vec{r}_i - \vec{R}_m(0)) \cdot \left[\frac{\partial \vec{R}_m(Q_K)}{\partial Q_K} \right]_{Q=0}}{|\vec{r}_i - \vec{R}_m(0)|^3} \quad (55)$$

where \vec{r}_i is the position of the i^{th} electron and $\vec{R}_m(Q_K)$ is the position of the m^{th} nucleus in the molecular frame. $\chi_{d_{XZ}}(\vec{r}_i)$ are the molecular orbital wavefunctions. There can be a contribution to the integral from only the region of the molecule for which the orbitals overlap. If $h^K(\vec{r}_i)$ is negligible in the overlap region, then the integral will vanish. In the present case the molecular orbitals are localized in different regions of the molecule, and the overlap region is small compared to the size of the molecule. That is, the region of integration in (54) is restricted to the metal-nitrogen bond region. In addition, the nuclei neighboring the overlap region are favored in the sum in (55). Unless there is a normal mode which involves considerable metal and nitrogen movement for a displacement along the normal coordinate, $\left[\frac{\partial \vec{R}(Q_K)}{\partial Q_K} \right]_{Q=0}$ will be small; $\langle d_{XZ} | h^K | e_{gX} \rangle$ will be small, since $h^K(\vec{r}_i)$ is small in the region of integration.

Totally symmetric vibrations which dominate the resonance Raman spectrum upon Band V excitation of Mn(III)EtioIX, are thought to originate from the A term, as is the case for resonance excitation in the Soret band. Therefore, no information concerning vibronic coupling in C_{4v} or D_{4h} symmetry groups is discernible from a_{1g} intensities with only Band V excitation. On the other hand, non-totally symmetric modes require interaction between excited electronic states and examination of Table 1 yields the following conclusions: (1) vibronic coupling between |C> and

$|D\rangle$ will result in a_{1g} (polarized) and a_{2g} (anomalously polarized) vibrations but not depolarized lines, and (2) to obtain depolarized lines, either $|B\rangle$ or $|Q\rangle$ must be present in $|V\rangle$ following configuration interaction.

One more point should be made. If, as Boucher has proposed, the donor orbitals are the next-to-highest filled π orbitals, then depolarized modes will vibronically couple pure charge transfer states, but anomalously polarized (a_{2g}) modes will not.

CHAPTER III

EXPERIMENTAL

The Samples

Manganese(III) Etioporphyrin I acetate was prepared⁸ by refluxing (4 hours) the etioporphyrin I free base in glacial acetic in the presence of air. Replacement of acetate by the thiocyanate was carried out in acetic acid/H₂O with excess KNCS present and the Mn(III)EtioNCS complex was crystallized from this solvent. The thiocyanate complex was synthesized by L. D. Spaulding. The Mn(III) etioporphyrin I iodide complex, prepared in the same manner using excess KI, was repeatedly recrystallized from a CH₂Cl₂/hexanes solution. The Cl⁻ complex was prepared by washing a CH₂Cl₂ solution of Mn(III)Etio(CH₃COO⁻) with aqueous HCl, followed by recrystallization from CH₂Cl₂-cyclohexane.

5,10,15,20-tetraphenylporphyrin Cr(III) chloride (Cr(III)TPPCl) was prepared by dissolving under nitrogen 1 gm of the free base porphyrin in 250 ml of N,N'-dimethylformamide. To this solution 500 mg of chromous acetate in 150 ml of DMF, prepared anaerobically, was added slowly as the temperature of the reaction mixture was raised to 100°C. The reaction was monitored spectrophotometrically until the Soret band of the free base had disappeared; it was then quenched by pouring the DMF solution onto ice. The metalloporphyrin was extracted with CH₂Cl₂, washed with water and taken to dryness. The porphyrin was chromatographed on neutral alumina with 1) benzene, and 2) 1% methanol in

CH_2Cl_2 . Percentage by weight for C,H,N, and Cl were calculated for CrTPPCl , $\text{CrC}_{44}\text{H}_{28}\text{N}_4\text{Cl}$: C,75.48; H,4.03; N,8.00; Cl,5.06; for $\text{CrTPPCl}\cdot\text{CH}_3\text{OH}$, $\text{CrC}_{45}\text{H}_{32}\text{N}_4\text{OCl}$: C,73.81; H,4.41; N,7.65; Cl,4.84. Elemental analysis gave the values C,74.24; H,4.33; N,7.91; Cl,5.03. The optical absorption spectrum agrees well with that reported by Gouterman et al.¹¹ The Cr(III)TPPCl sample was prepared by L. D. Cheung.

The Raman Scattering Apparatus

The spectra were obtained with the standard Raman scattering arrangement shown in Figure 7. The apparatus consists of (1) an excitation source and optics for preparing the incident beam characteristics, (2) the sample, (3) the optics for collecting the scattered light, (4) the spectrometer and detector, and (5) the photon counting and data storage electronics. With the exception of one spectrum taken with the Georgia Tech School of Chemistry Kr^+ laser and Raman scattering apparatus, all spectra were taken with the School of Physics Raman scattering apparatus.

The exciting radiation sources were provided by a Coherent Radiation (Model 52) Argon ion laser, a Krypton ion laser (Model 500K), and an Ar^+ laser-pumped Spectra Physics dye laser (Model 390). The Ar^+ laser had an output of 1.2 watts (at 28 amperes) at 514.5 nm polarized vertically with respect to the laboratory. Later, the CR-2 Ar^+ laser tube was replaced by the CR-3 tube; the output power at 514.5 nm was 1.4 watts (at 28 amperes). The dye laser power with Rhodamine 6G as the fluorescent dye was typically 200 mw at 580.0 nm when pumping at

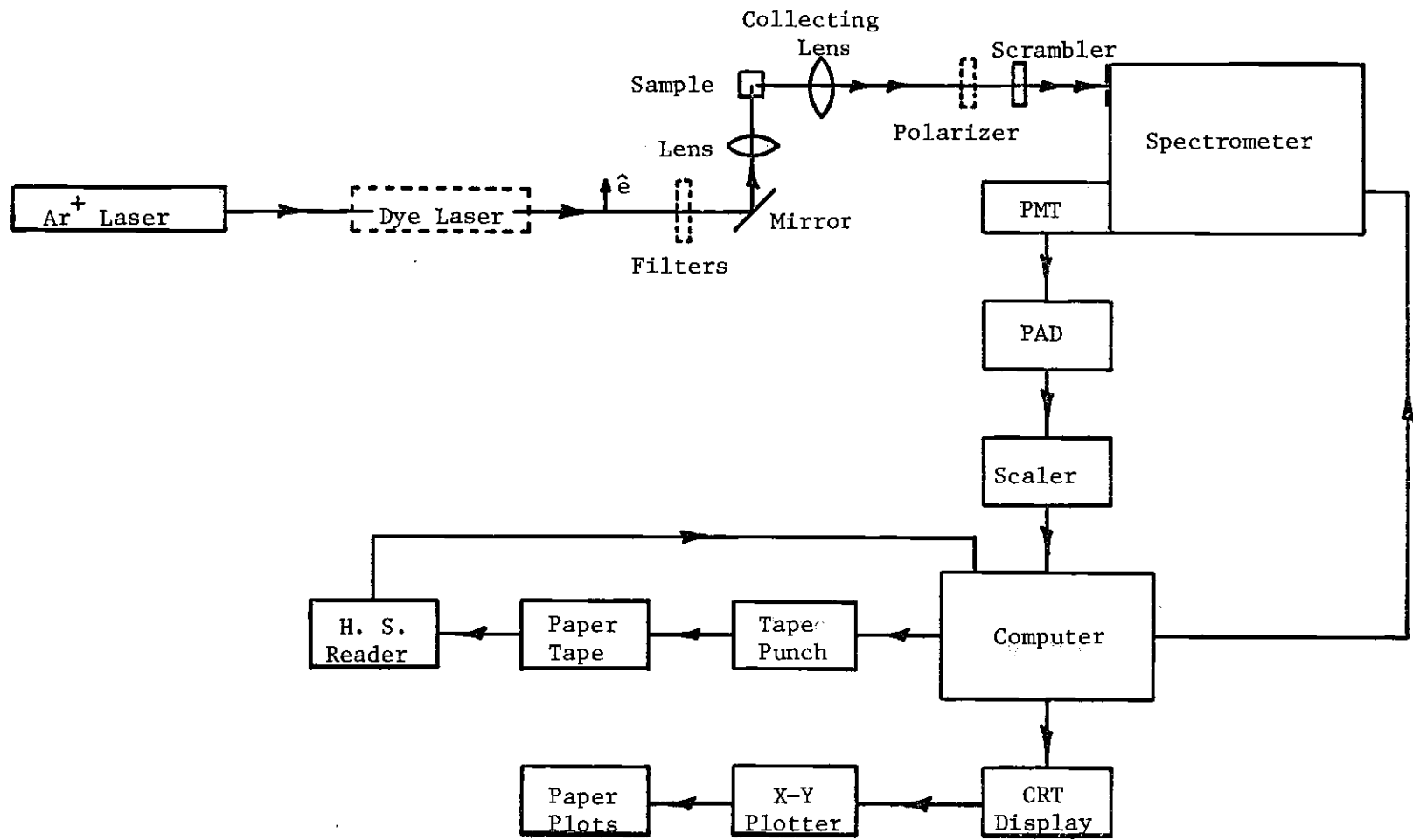


Figure 7. Raman Scattering Apparatus

2 watts for all lines of the Ar⁺ laser.

The incident laser beam was directed through narrow band interference filters (FWHM = 10 nm) to remove plasma emission lines, originating from the laser tube, and residual pumping radiation from the dye laser beam. In addition, a 560.0 nm sharp cut (short wavelength absorbing, long wavelength transmitting) filter was needed to remove pump laser radiation. For some laser lines neutral density filters reduced the incident power below 200 mw to avoid local heating and photodecomposition of the colored samples.

The prepared laser beam, initially horizontal, was directed upward by a mirror, focused into the sample by a 60 mm focal length lens located above the mirror, and the scattering column aligned parallel to the vertical entrance slit of the spectrometer. The rotating sample cell and collecting optics for 90° scattering geometry is shown in Figure 8. For solution samples the rotating cell (Figure 8) was a 3/4" diameter pyrex glass cell fabricated by Dell Optics. The upper portion of the cell was solid except for a small central channel so that the spinning liquid was confined to the lower portion allowing small volumes to be analyzed (typically <1 ml). A Teflon stopper and silicone vacuum grease sealed the cell to prevent a change in concentration through evaporation. The cell was retained in a brass holder by two O-rings. The cell, rotated at 3400 rpm by an AC motor, was positioned so that the scattering column was in the solution approximately 0.15 mm from the cylindrical surface of the cell. The error in positioning the cell is less than 0.10 mm.

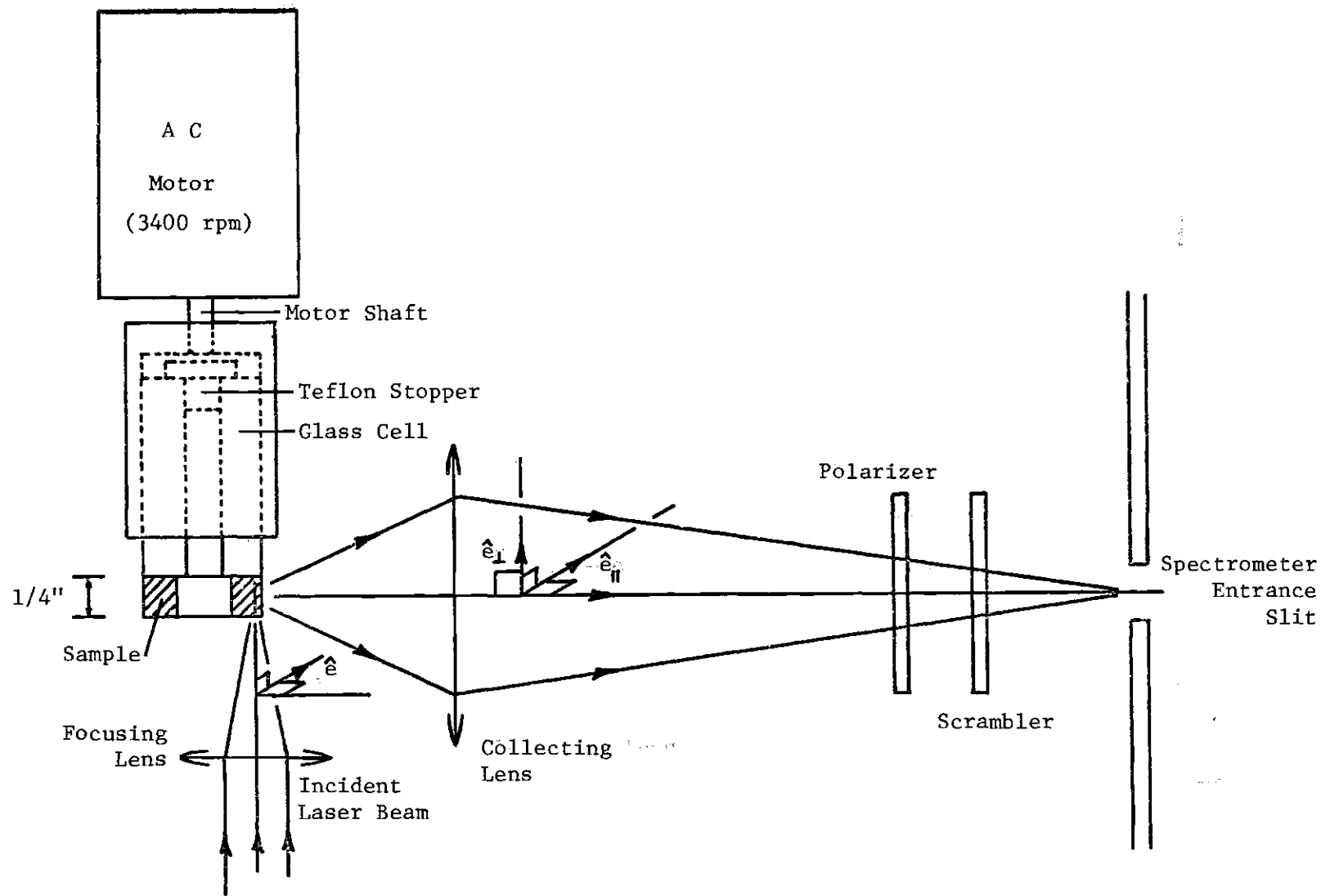


Figure 8. Standard Raman Scattering Arrangement: 90° Scattering Geometry (Rotating Cell is Shown.)

Solid sample pellets were rotated on a 3/4" diameter aluminum platform. The sample pellets (typically 1/2" in diameter and 2 mm thick) were held in place by a Teflon retainer which slipped snugly over the outside of the platform. The sample was exposed through a 3/8" diameter hole in the retainer and oriented so that the incident beam and the surface of the pellet formed a 10° angle.

The scattering column was imaged on the entrance slit of the spectrometer by the collecting lens. A polarization scrambler, placed in front of the entrance slit, insured the response of the spectrometer and detector would be independent of the polarization of the scattered light. For some spectra the scattered light was analyzed into its parallel ($I_{||}$) and perpendicular (I_{\perp}) components with respect to the incident polarization by a polarizer (HN-22 Polaroid sheet) placed between the collecting lens and the scrambler.

The spectrometer was a 3/4 meter Spex Czerny-Turner double monochromator (Model 1401). Two monochromators were necessary to reduce the Rayleigh scattered component sufficiently to observe the Raman spectrum. The replica gratings had 1200 grooves/mm and were blazed at 500.0 nm. The instrument dispersion was 0.55 nm/mm. Typical entrance, intermediate, and exit slit widths were 250, 250, and 250 microns, and the entrance slit height was 10 mm for solution samples. For solid samples typical slit widths were 400, 400, 400 microns, and the entrance slit height was 5 mm.

Scattered light from the exit slit of the spectrometer was detected by an ITT Startracker (Model FW 130) photomultiplier tube (PMT)

with an effective photocathode surface of rectangular shape (10 mm x 2 mm). The PMT had an extended red sensitivity surface (S-20) and was operated at -1500 volts by a Tennelec (Model AEC-100) power supply. By cooling to -20°C with a Products for Research (Model TE-104) thermoelectrically refrigerated chamber, the PMT dark count was lowered from 120 counts/sec at room temperature to 3 counts/sec.

The pulses from the PMT formed the input of a Nuclear Data (model 520) preamplifier-amplifier-discriminator (PAD) unit. Input pulses above a threshold determined by the discriminator setting trigger uniform 1 usec pulses. These pulses were counted by a dual scaler constructed at the School of Physics for this purpose.

Data acquisition and spectrometer operation were controlled by a Digital Equipment Corporation (Model PDP 8/f) computer. A spectrum was obtained by counting pulses from the PAD for specified time intervals (typically 1-5 sec). At the end of the time interval the number of pulses accumulated by the scaler was stored in computer memory, and simultaneously displayed on a Tektronix (Model 604) oscilloscope. The computer then generated the pulses required for a stepping motor to increment the gratings (1 cm^{-1} /increment), the scaler was cleared, and counting restarted. Up to 2048(4 quadrants) of data points could be stored and displayed.

Spectra could be stored graphically and digitally. Spectra were plotted on a Metagraphics x-y plotter interfaced to the computer, and punched onto paper tape for permanent storage. The spectra could then be retrieved via a high speed reader for use with the data manipulation

and analysis programs available. The necessary programs were written by Kenneth Everett.

Methods

Exciting lines from the Ar^+ and Kr^+ lasers were employed in the study of Band V of the NCS^- and I^- Mn(III)EtioI complexes. Exciting frequencies 560.0 nm to 620.0 nm in the region of Bands III and IV were provided by the Rhodamine 6G dye laser.

Resonance Raman spectra of Mn(III)EtioCl were obtained for irradiation at frequencies near Bands III and IV. The sample was a single pressed pellet of ≈ 2 mg of Mn(III)EtioCl in a 3:7 mixture of Na_2WO_4 and KBr . The sodium tungstate was included to provide a standard ($934 \text{ cm}^{-1} \text{ WO}_4^{2-}$ line) for the incident light intensity at the sample.

The pellet was constructed by grinding the mixture with an agate mortar and pestel until a uniform fine powder was attained. The mixture was then pressed in a standard 1/2" diameter infrared pellet die for two minutes at $19,000 \text{ lbs/in}^2$ pressure.

During recording of the spectra a stream of dry N_2 prevented deterioration of the deliquescent pellet. This solid sample was required since solutions of the manganese complexes fluoresced weakly at the dye laser wavelengths. Repeated attempts to purify the porphyrin by recrystallization did not appreciably reduce the fluorescence.

When excited in the vicinity of Band V, however, Mn(III)EtioX , $\text{X}^- = \text{MCS}^-$, and I^- , dissolved in CHCl_3 , CDCl_3 , CH_2Cl_2 , or CS_2 did not exhibit interfering fluorescence. The solvents provided reference lines in the Raman spectra at 1220 cm^{-1} (CHCl_3), 908 cm^{-1} (CDCl_3),

287 cm^{-1} (CH_2Cl_2) and 802 cm^{-1} (CS_2). The concentration was 10^{-4} - 10^{-5} molar.

No decomposition was noted in the solid and solution samples of MnEtioX , $\text{X}^- = \text{Cl}^-$, NCS^- . Decomposition of CrTPPCl or MnEtio was noted with laser irradiation in air saturated samples. The decomposition appears to be photooxidation, and irradiation of anerobic samples followed by measurement of the electronic absorption spectra showed no or minimal changes under these conditions. Even with these precautions a slow alteration of the optical absorption spectrum of the iodide complex was observed.

The Cary (Model 14) spectrophotometer was employed for the absorption spectra.

CHAPTER IV

RESULTS

Raman Spectra

Resonance Raman spectra of Mn(III) etioporphyrin complexes were obtained for the purpose of constructing excitation profiles for selected Raman lines. The spectra required are $I_{\text{TOTAL}} = I_{||} + I_{\perp}$ (taken without the polarizer); in addition, $I_{||}$ and I_{\perp} Raman spectra provided the polarization properties of the Raman lines. In this section typical Raman spectra of Mn(III)EtioIX obtained under various excitation conditions are displayed (Figures 9,10,11,12) and the qualitative features of the spectra are discussed. In the next section the experimental excitation profiles for selected Raman lines are presented.

The resonance Raman spectrum of Mn(III)EtioICl in a 30% Na_2WO_2^- KBr pellet, displayed in Figure 9, is typical of spectra obtained when the exciting frequency resides in Bands III and IV. For samples in pellet form, the depolarization ratio of a Raman line is not quantitatively reliable due to scrambling of the polarization by the solid matrix; however, the depolarization ratio is accurate enough to determine the symmetry of most of the vibrations by inspection of the $I_{||}$ and I_{\perp} intensities for the line. For the 1313 cm^{-1} line in Figure 9, I_{\perp} is greater than $I_{||}$ (using peak heights); therefore, ρ for this line is greater than one and the line is anomalously polarized. It is concluded from these depolarization ratios that non-totally symmetric modes dominate the Band III and IV Raman spectra.

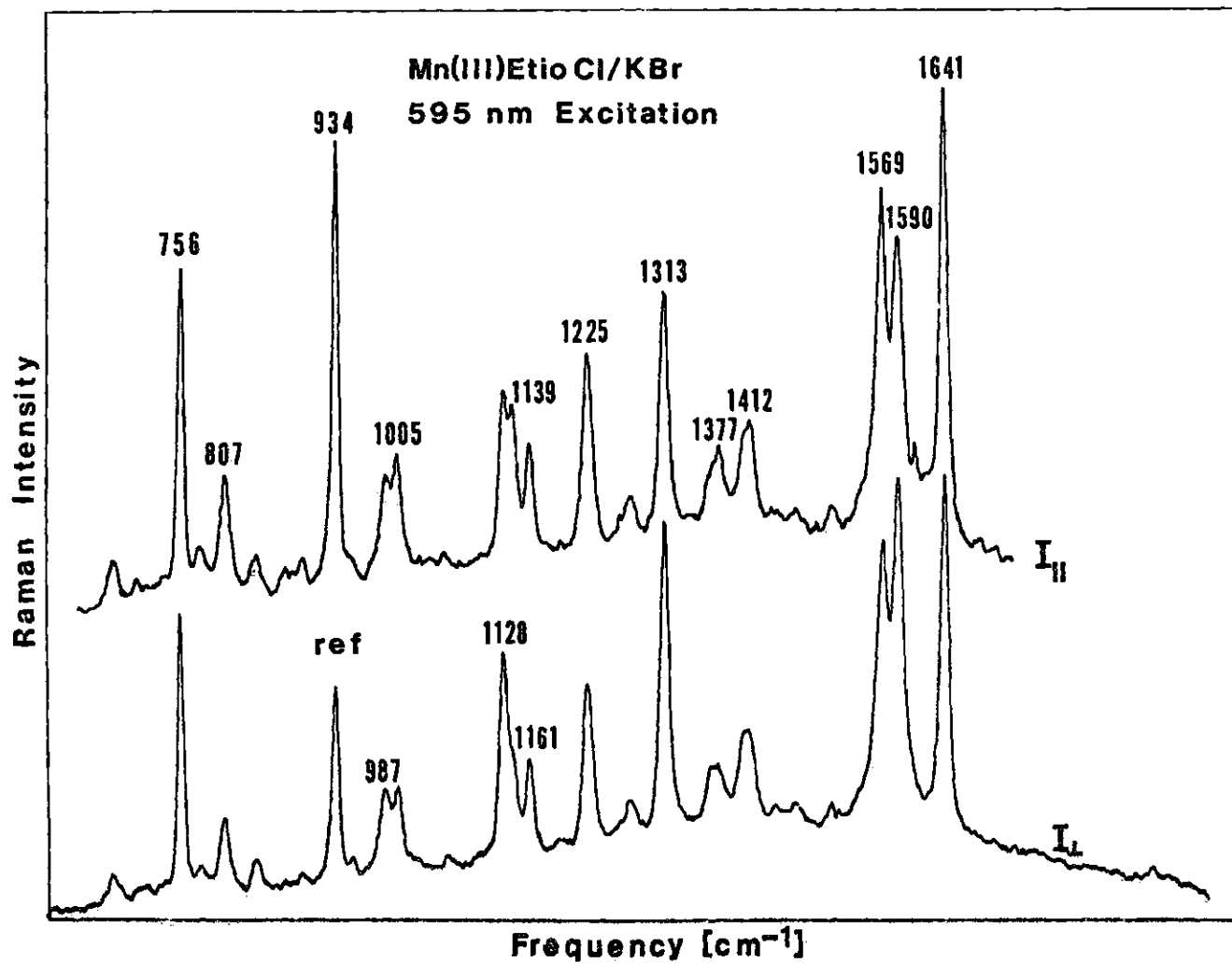


Figure 9. Resonance Raman Spectrum (I_{II} and I_I) of Manganese(III) Etioporphyrin I Chloride in KBr: Typical of Band III and IV Raman Spectra

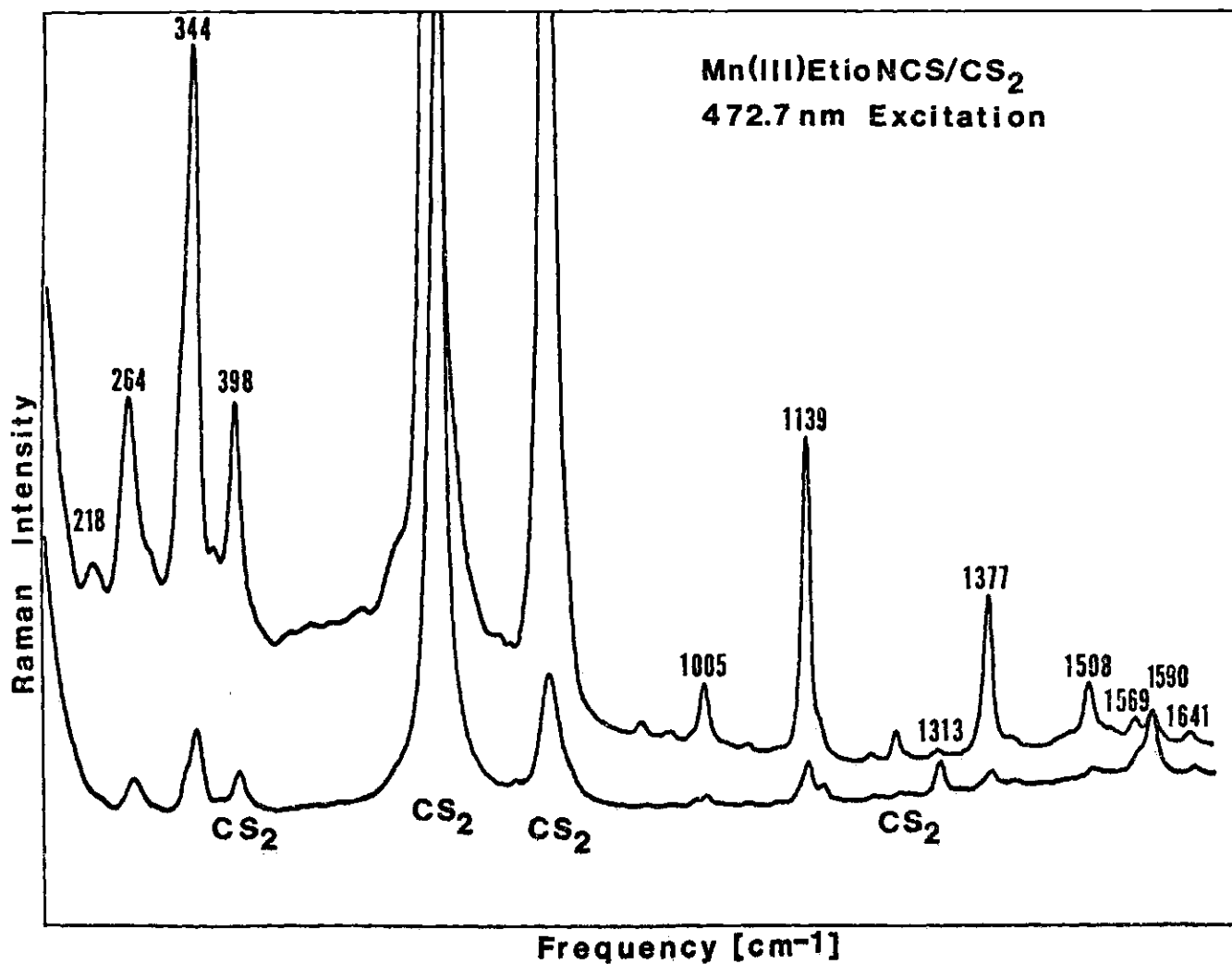


Figure 10. Resonance Raman Spectrum (I_{\parallel} and I_{\perp}) of Manganese(III) Etioporphyrin I Thiocyanate in Carbon Disulfide: Typical of Band V Raman Spectra

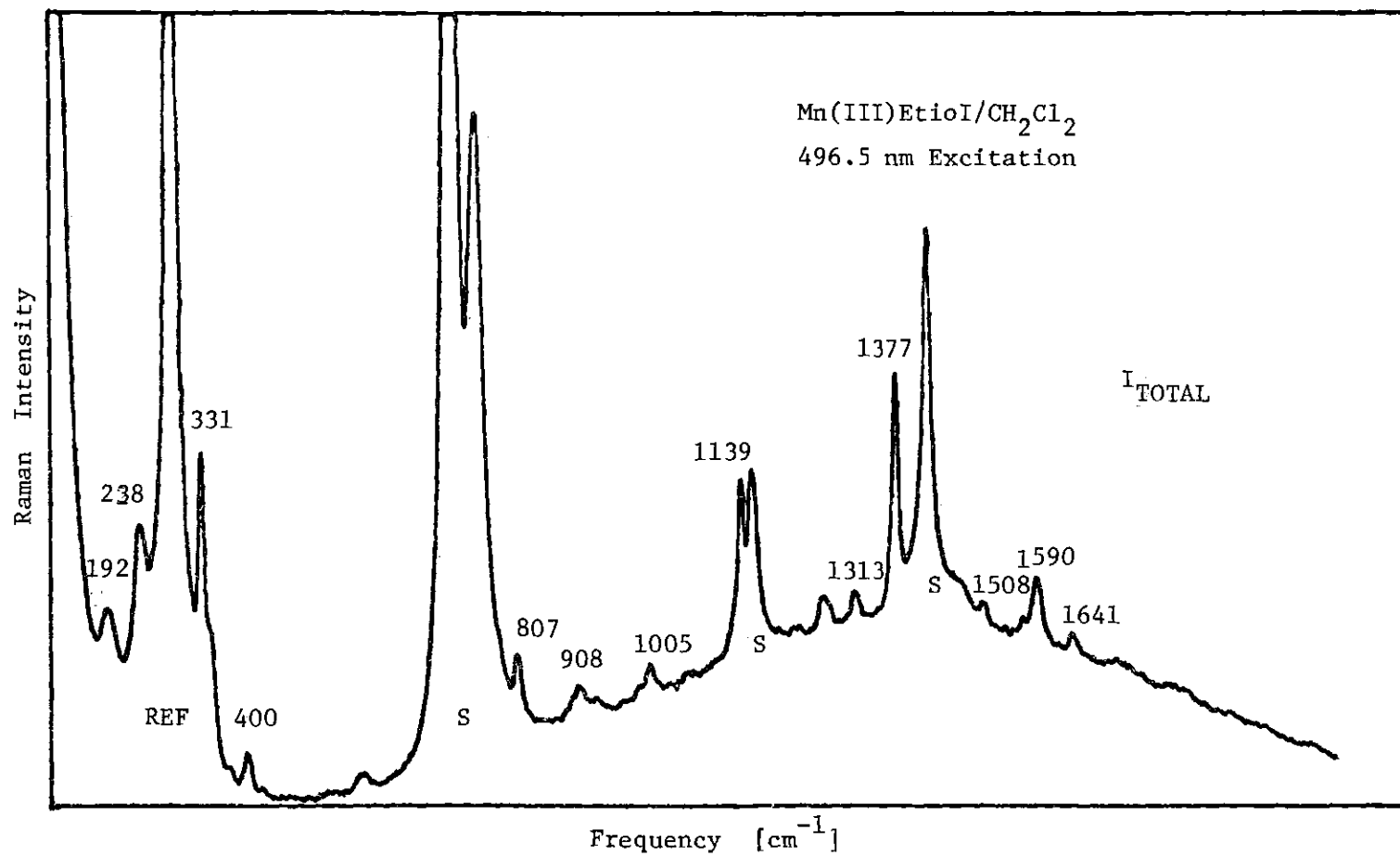


Figure 11. Resonance Raman Spectrum (I_{TOTAL}) of Manganese(III) Etioporphyrin I Iodide in Carbon Disulfide: Typical of Band V Raman Spectra

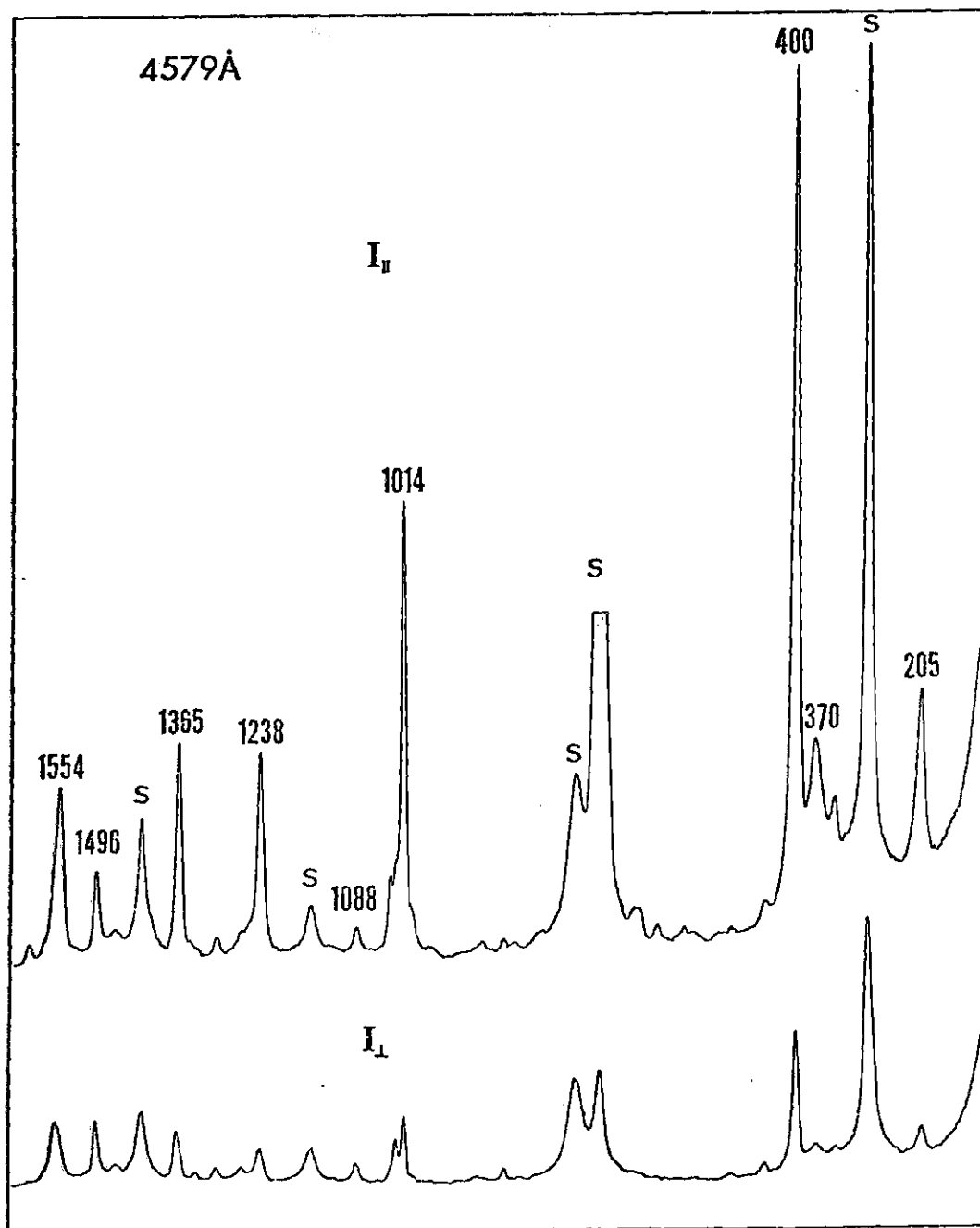


Figure 12. Resonance Raman Spectrum (I_1 and I_2) of Chromium(III) Tetrphenyl Porphyrin in Methylene Chloride: Excitation at 457.9 nm Near B-Band(Band V) Maximum

Upon excitation in the Band V region of the Mn(III)EtioI thiocyanate and iodide complexes in solutions, (Figures 10 and 11, respectively) the polarized lines are dominant. However, some weaker depolarized and anomalously polarized lines are noted. A single Raman spectrum of Cr(III)TPPCl was obtained by Duncan Cheung. Figure 12. Excitation was at 457.9 nm well into the strong B band peak at 448 nm in CH_2Cl_2 . Here the totally symmetric modes completely dominate the Raman spectrum. Only one possible depolarized mode is observed at 1496 cm^{-1} .

Excitation Profiles

Raman line intensities relative to solvent peak heights (except for Mn(III)EtioICl spectra, where integrated intensities were employed instead) were obtained from graph paper plots of the spectra. These relative Raman intensities were first corrected⁵³ for chromophore absorption of the scattered light by multiplying by the correction factor, $10^{-(A_{\text{REF}} - A_{\text{R.L.}})x}$, where x is the path length of the scattered light in millimeters, and A_{REF} and $A_{\text{R.L.}}$ are the absorbance (1 mm cell) for the solvent reference line and porphyrin Raman line, respectively. Finally, the relative Raman intensities were further corrected for response of the Raman scattering apparatus. The response curve, obtained by a method⁵⁴ based on the theoretically calculated intensities of the rotational Raman lines of D_2 , provided a second correction factor. Excitation profiles were constructed by plotting the corrected relative Raman line intensities versus the frequency of the exciting radiation.

Band III and IV excitation profiles of selected vibrations are shown in Figure 13. For polarized and depolarized lines, intensities

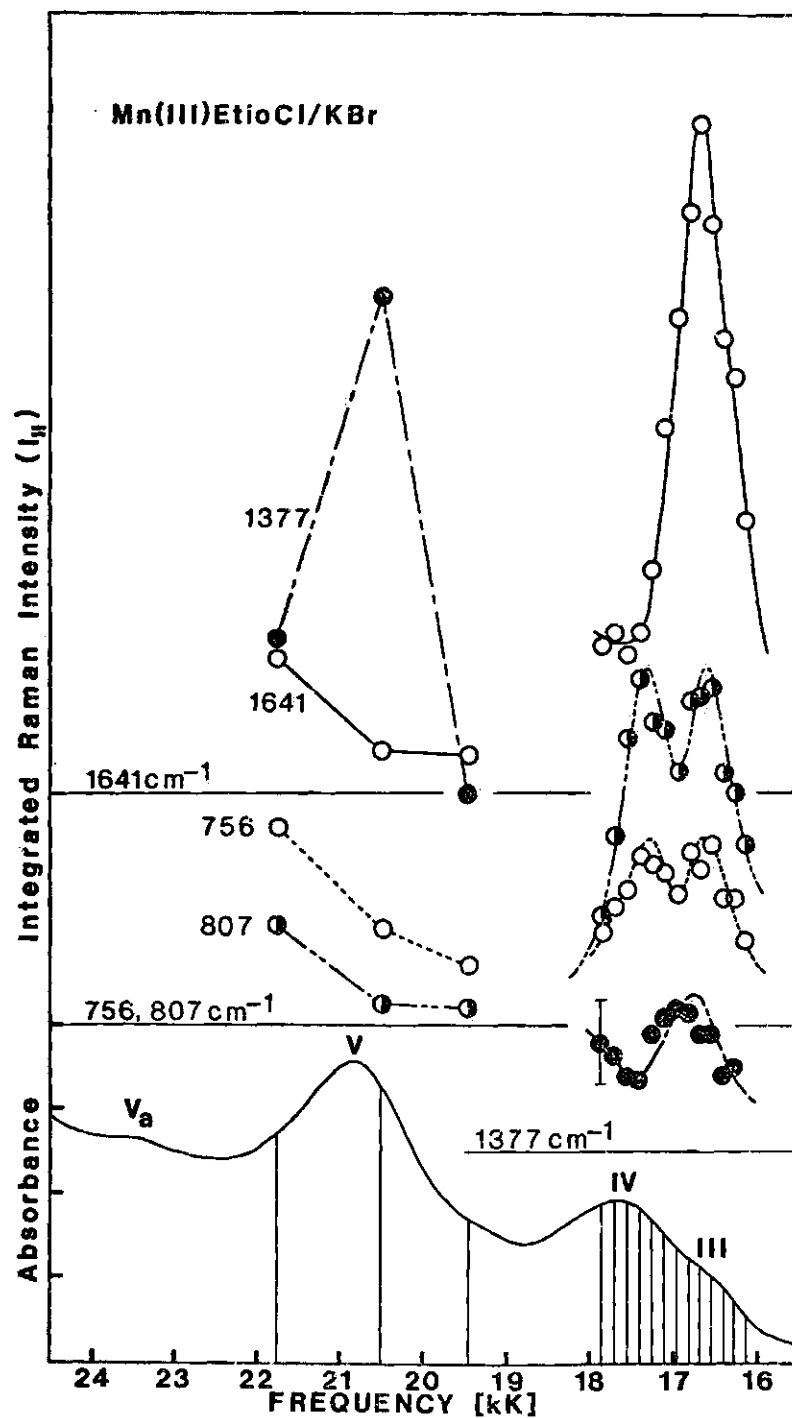


Figure 13. Manganese(III) Etioporphyrin I Chloride Excitation Profiles and Absorption Spectrum in KBr

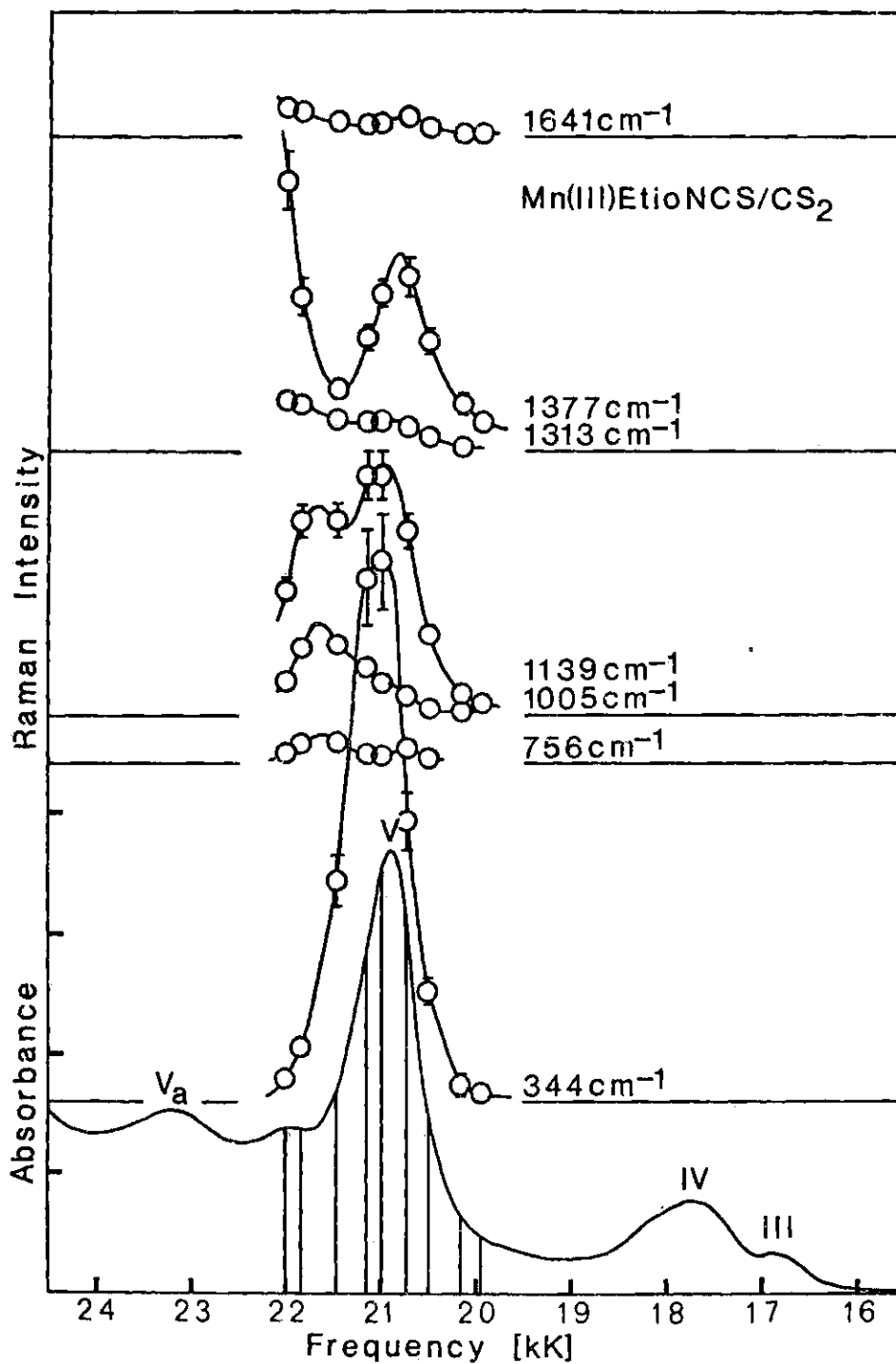


Figure 14. Manganese(III) Etioporphyrin I Thiocyanate Excitation Profiles and Absorption Spectrum in Carbon Disulfide

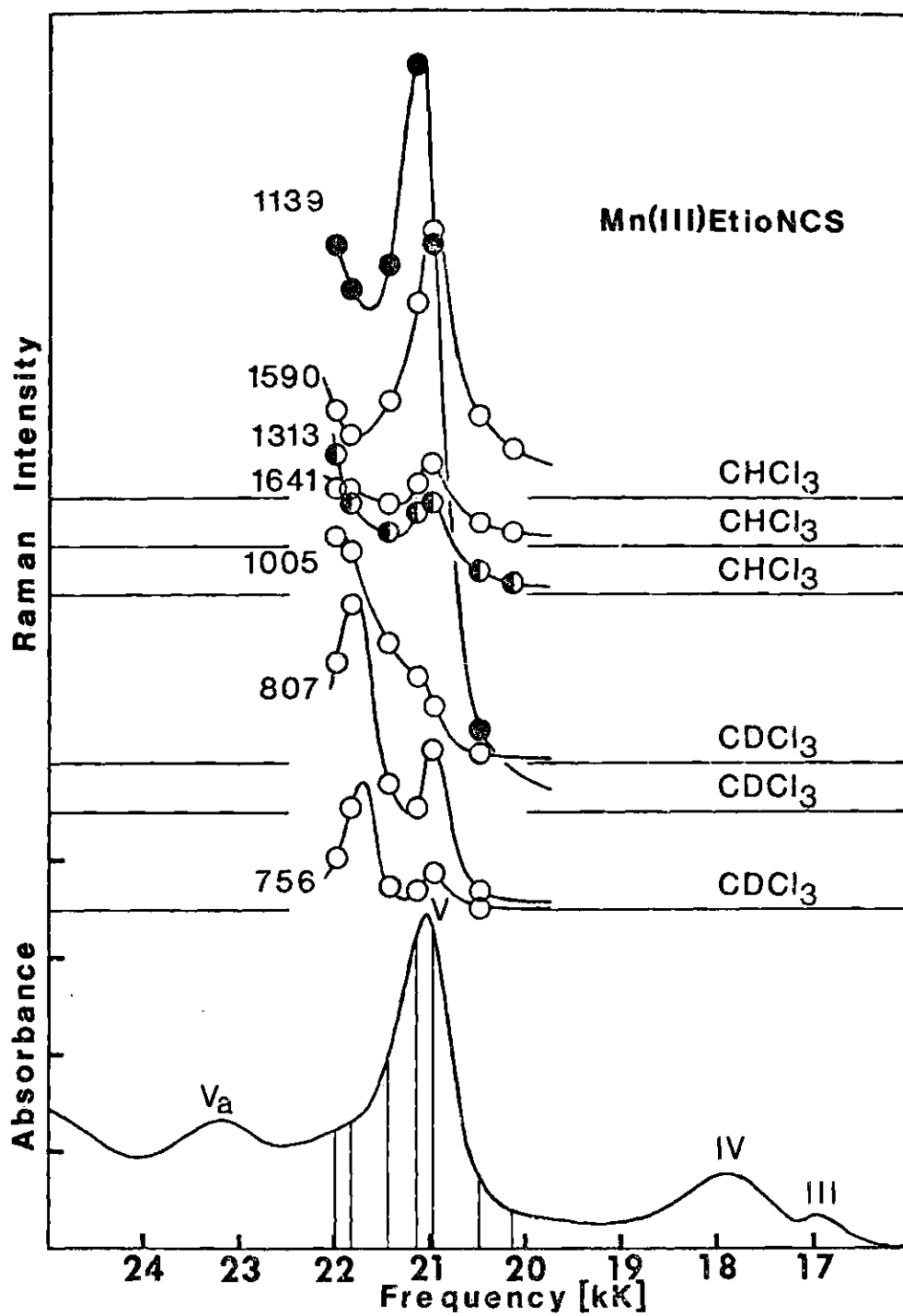


Figure 15. Manganese(III) Etioporphyrin I Thiocyanate Excitation Profiles and Absorption Spectrum in CHCl₃ or CDCl₃

plotted are $I_{||}$, since I_{\perp} intensities peak at the same exciting wavelength. An initial maximum in the excitation profile is noted at the shoulder identified as Band III in the electronic absorption spectrum in KBr, and secondary peaks are observed for the 756 (dp) and 807 (p) cm^{-1} vibrations. A secondary maximum is one that occurs at the frequency of the first maximum plus the vibrational mode frequency. Secondary peaks presumably are present for the higher frequency vibrations, but lie outside the region of available laser frequencies.

Band V excitation profiles of the 344 (p), 756 (dp) 807 (p), 1005 (p), 1139 (p), 1313 (?, ap), 1377 (p), 1590 (p,ap) and 1641 (dp) cm^{-1} resonance Raman lines are displayed in Figures 14 and 15 for the NCS^- complex of Figure 16 for the I^- complex. Initial peaks in the excitation profiles are close to the electronic absorption maximum of Band V. The 344 cm^{-1} profile is shifted toward higher energies which points to an unresolved secondary maximum. The shoulder on the 331 cm^{-1} profile in Figure 16 is ascribed to an impurity formed during irradiation. We believe the impurity is a Mn(III) porphyrin complex with its Band V at 473 nm (21.1 kK). For the thiocyanate complex definite secondary maxima for the 756, 807 and 1005 cm^{-1} lines are observed, but other secondary peaks appear to be outside the available laser irradiating frequencies, since the scattered intensity does increase toward higher energies for vibrations whose frequencies are $\geq 1100 \text{ cm}^{-1}$. These secondary peaks reside in the high energy shoulder of Band V located at 21,800 cm^{-1} (not Band V_a). For the I^- complex the secondary maxima are observed for the 1139 (p) cm^{-1} , 1313 (ap) cm^{-1} , and 1377 (a) cm^{-1} lines in addition to those noted in the NCS^- complex.

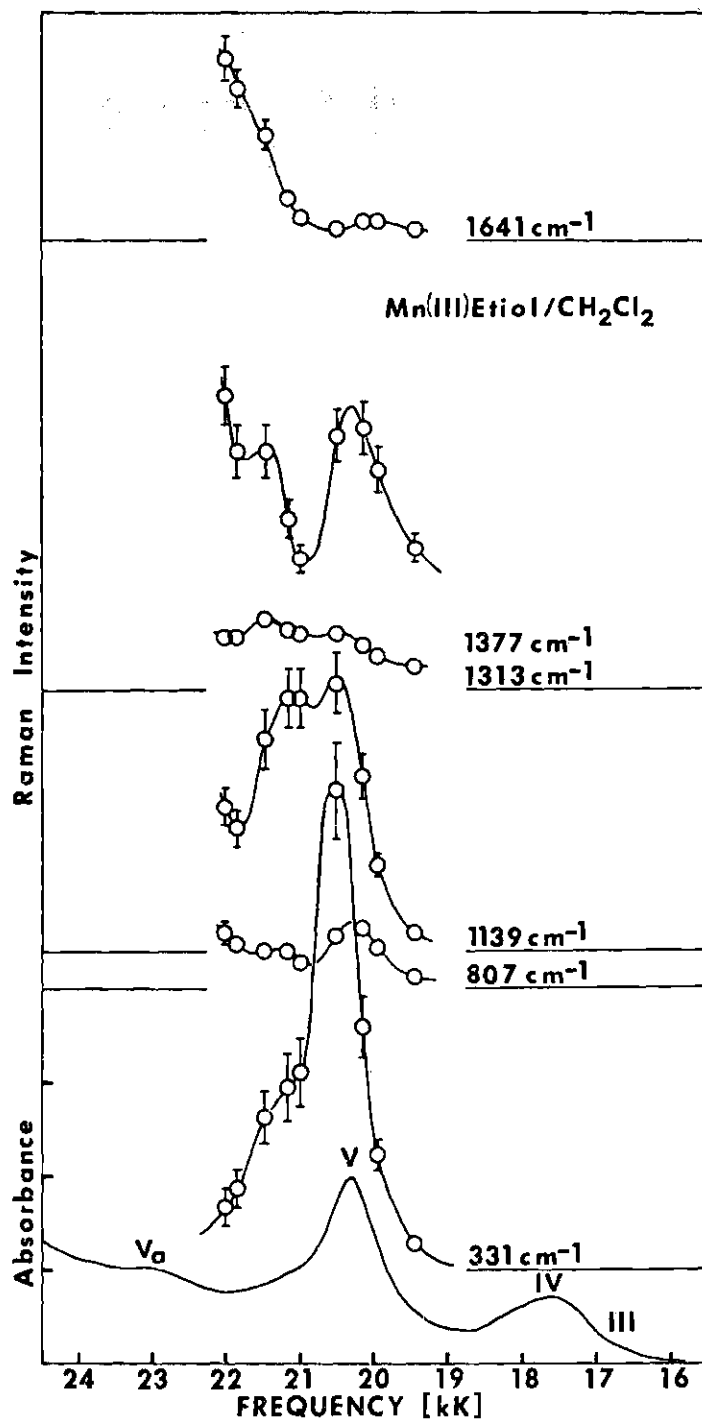


Figure 16. Manganese(III) Etioporphyrin I Iodide Excitation Profiles and Absorption Spectrum in Methylene Chloride

CHAPTER V

DISCUSSION AND CONCLUSIONS

Introduction

The resonance Raman study of Mn(III) porphyrins has produced interesting results in three areas. (1) Electronic transition assignments can be made for several of the bands in the optical absorption spectrum. (2) The non-adiabatic correction to the crude Born-Oppenheimer states is shown necessary to explain the dependence of the Raman intensity on exciting frequency in the region of Bands V and V_a . In addition, the results represent the first experimental verification of the large difference in the resonance scattering intensity at the 0-0 and 0-1 frequencies which is a consequence of the non-adiabatic vibronic coupling term in the Raman scattering tensor (16). (3) Finally, evidence of vibronic coupling by totally symmetric vibrational modes is presented.

In the next two sections electronic band assignments for Bands III, IV, and V are proposed on the basis of the resonance Raman data. Also, the question of selective enhancement of low frequency modes containing metal-ligand contributions is considered. In the third section, an interpretation of the Mn(III) TPPX resonance Raman data is tentatively proposed. In the final section, the unique frequency dependence of excitation profiles in the region of Band V and V_a are shown to imply non-adiabatic (D-term) coupling contributions to the Raman scattering,

and, as a consequence, Band V_a may be assigned to an electronic transition, also.

Electronic Assignments for Bands III and IV

It is proposed that Bands III and IV of Mn(III) porphyrin absorption spectra are the 0-0 and 0-1 components of the Q band, respectively, based on the following evidence. (1) The separation between Bands III and IV is $\approx 1000 \text{ cm}^{-1}$, a value slightly smaller than that found in typical metalloporphyrins, but nonetheless consistent with identification of Band IV as the vibrational satellite of Band III. (2) Dominance of non-totally symmetric modes in the Band III and IV Raman spectra provides strong support that these bands arise from $\pi \rightarrow \pi^*$ excited states vibronically coupled to dipole allowed states. The same feature is noted in Q band resonance Raman spectra of metalloporphyrins with typical absorption spectra. (3) The frequency dependence of the scattered intensity is analogous to Q band excitation profiles of nickel⁵⁵ or copper⁵⁶ porphyrins. Maxima in the excitation profiles at Band III indicate it is the 0-0 component of the Q band. For the 756 (dp) and 807 (p) cm^{-1} lines secondary maxima in the excitation profiles are observed at the 0-1 frequency. This is consistent with our assignment of Band IV. Boucher⁸ considered assignments of Bands III and IV to the 0-0 and 0-1 components of the Q state, but concluded that the $\sim 1000 \text{ cm}^{-1}$ separation of absorption maxima was smaller than in normal spectra, and the appearance of a terms in both Band III and IV MCD spectra were inconsistent with this assignment. In this connection we note that vibronic interaction of excited states results in a non-uniform shift in the vibrational levels,

such that in the lower excited state the 0-1 level is shifted more to lower energy than is the 0-0 level.⁴⁰ Applying this result, a nearby allowed state V and the 0-0 and 0-1 Q states are repelled, and the separation between the 0-0 and 0-1 Q band maxima is reduced. Additionally, *a* terms of comparable molar ellipticity for both 0-0 and 0-1 Q bands are observed in the MCD spectrum of Zn(II) TPP—a species exhibiting a typical metalloporphyrin absorption spectrum.⁵⁷

Electronic Assignment for Band V

It has been proposed^{8,9} that Band V of Mn(III) porphyrin absorption spectra has both charge transfer and $\pi \rightarrow \pi^*$ character. The charge transfer character is inferred from the presence of extra absorption bands and is based on theoretical predictions⁵⁰ that porphyrin-to-metal charge transfer transitions will occur in the visible. The $\pi \rightarrow \pi^*$ character was adduced from the extinction coefficient which is a factor of 2-10 larger than that for normal Q bands ($\epsilon_Q \sim 1.5 - 2.5 \times 10^3$ liter/mole-cm).¹ The added intensity of a charge transfer Band V presumably arises from a dipole allowed $\pi \rightarrow \pi^*$ contribution, i.e., $|B\rangle$. A similar conclusion was reached in a resonance Raman study of charge transfer bands in heme proteins.⁴³ We also assign Band V to a state with both charge transfer and $\pi \rightarrow \pi^*$ character for these reasons, and we have proposed a model (Chapter II) for these states based on configuration mixing of the $\pi \rightarrow \pi^*$ and charge transfer states.

It has been suggested that the apparent enhancement of low frequency a_{1g} modes can be interpreted as indicating charge transfer character. However, the theoretical considerations in Chapter II suggest that low frequency enhancement will not be observed in porphyrin systems.

Enhancement of totally symmetric modes relative to non-totally symmetric vibrations is a direct consequence of increased dipole strength in Band V compared to the Q band. The Raman intensity originating from the A term will increase as ϵ_V^2 , whereas the Raman intensity of Herzberg-Teller modes will increase as ϵ_V . To emphasize the independence of polarized mode enhancement from charge transfer character, we have examined the resonance Raman spectrum of Cr(III)TPPCl with 457.9 nm excitation. This metalloporphyrin has a strong B absorption peak at 448 nm in CH_2Cl_2 , so excitation is well into the absorption. Comparison of this spectrum, shown in Figure 12, with that of Mn(III)EtioNCS in Figure 10 substantiates the claim that enhancement of a_{1g} vibrations is not indicative of charge transfer. Moreover, the Raman spectrum of Cr(III)TPPCl does not exhibit scattering from non-totally symmetric modes, (excepting the 1496 (dp) cm^{-1} vibration) while lines at 1641 (dp), 1590 (ap, p), 1313 (ap,?) and 756 (dp) cm^{-1} are displayed in the manganese complex spectrum. The conclusions of Chapter II can be used now as evidence in favor of both $|B\rangle$ and $|Q\rangle$ character in state V. Again $|B\rangle$ character is indicated by the large extinction coefficient observed for $|V\rangle$, and $|Q\rangle$ character is adduced from the presence of both anomalously polarized (a_{2g}) and depolarized (b_{1g} and b_{2g}) modes in Band V Raman spectra. The non-totally symmetric modes arise from Q-B vibronic coupling of $|V\rangle$ with states at higher energy which are probably predominately composed of $|B\rangle$ and charge transfer contributions. Thus $|V\rangle$ must contain $|Q\rangle$ contributions as well as $|B\rangle$. Gaughan *et al.*⁷ previously noted non-totally symmetric vibrations in Mn(III)TPPX (X⁻ = Cl⁻, Br⁻, I⁻) complexes and concluded that state V was coupled vibronically to other electronic states.

It is suggested that selective enhancement of low frequency modes is not observed in Mn(III) or Cr(III) complexes. Omitting the vibration at 331 cm^{-1} in Mn(III)EtioI, 344 cm^{-1} in Mn(III)EtioNCS, or 400 cm^{-1} in Cr(III)TPPCl, the low frequency modes do not appear significantly enhanced over the high frequency a_{1g} modes. The very intense Raman line in the $300\text{--}400\text{ cm}^{-1}$ region observed in most metalloporphyrins, is assigned as a strong Frank-Condon mode. This view is supported by MCD spectra of the Q band of metalloporphyrins which show a Frank-Condon vibration at approximately this frequency.⁵⁷ Also in CuEtioI the 342 cm^{-1} mode is already quite strong even in the Q band where Herzberg-Teller modes dominate the resonance Raman spectra. Apparently, the vibration is also strongly Frank-Condon allowed in Band V of Mn(III) porphyrin complexes and in the Soret band of Cr(III) porphyrin complexes.

Mn(III)TPPX Resonance Raman Data

Gaughan et al.⁷ noted an increase in scattering intensity upon excitation into Band V for the non-totally symmetric modes relative to the polarized modes when the Cl^- and Br^- complexes are compared to Mn(III)TPPE complex. It is apparent from their data that the $887(\text{p})\text{ cm}^{-1}$ polarized vibration also exhibits increased Raman scattering. The assignment of the electronic states in Mn(III) porphyrins proposed here suggests an interpretation of this anion effect. (1) The B content of the state V is reduced for the I^- complex with concomitant increase in Q and charge transfer character. Reduction of the B contribution also accounts for the decrease in the absorption intensity of Band V for the I^- complex. The extinction coefficient for Band V in the Cl^- and Br^- Mn(III)TPP complexes is 7.7×10^4 and 9.0×10^4 liter/mole-cm, respectively, and

that for the I^- complex is only 4.3×10^4 liter/mole-cm, roughly equal to the extinction coefficient for Band V_a.⁴ (2) The decreased Band V transition dipole favors modes which mix $|V\rangle$ with $|V_a\rangle$ and $|VI\rangle$. Indeed, marked enhancement relative to other polarized modes is noted for the 887(p) cm^{-1} and 1534(ap) cm^{-1} vibrations of Mn(III)TPPI. Since a_{1g} and a_{2g} symmetry perturbations are most effective (Table I) in mixing C and D, we suggest that only in this way do the resonance Raman data support increased charge transfer character for Band V of the Mn(III)TPPI absorption spectrum.

Band V and V_a Excitation Profiles

The excitation profiles in the region of Band V and approaching V_a exhibit unusual behavior. The profiles for many lines where the 0-0 and 0-1 maxima are resolved show greater intensity at the 0-1 frequency. (See Figure 14, 15, and 16.) This behavior can be explained by considering non-adiabatic coupling contributions to resonance Raman scattering from states V and V_a.

Near and at resonance the Herzberg-Teller (B) and non-adiabatic (D) contributions to the scattering tensor (16) will be,⁵⁸

$$(B + D)_{\rho\sigma}^{*ijK} \sim h_{ij}^K \left[\frac{M_{ig}^{\rho} M_{jg}^{\sigma}}{E_{i0} - E_{g0} - h\nu - i\Gamma_{i0}} \left\{ 1 + \frac{h\nu_i^K}{E_{i0} - E_{j1}} \right\} + \frac{M_{ig}^{\sigma} M_{jh}^{\rho}}{E_{i1} - E_{g0} - h\nu - i\Gamma_{i1}} \left\{ 1 - \frac{h\nu_j^K}{E_{i1} - E_{j0}} \right\} \right] \quad (56)$$

for $|i\rangle = |V\rangle$ and $|j\rangle = |V_a\rangle$. Equation (56) is arrived at by arguments similar to those leading to (38) for the B term alone. The plus sign in

(56) holds for a_{1g} , b_{1g} , and b_{2g} vibrations, whereas the minus sign holds for an a_{2g} vibration. Since $|E_{V_a 1} - E_{V_0}| > |E_{V_a 0} - E_{V_1}|$, the last term in (56) is largest; therefore, the non-adiabatic contribution (the last term in the curly brackets) provides unequal Raman intensities for excitation at the 0-0 and 0-1 frequencies. At the 0-1 frequency the non-adiabatic contribution is large and adds to the Herzberg-Teller contribution. On the other hand at the 0-0 frequency the non-adiabatic contribution is smaller and reduces the 0-0 Raman intensity. It is noted that the difference in the 0-0 and 0-1 intensities will be enhanced for high frequency vibrations.

The pronounced peak at the 0-1 frequency cannot be explained by A or B terms but must involve the D term. The B term alone gives equal 0-0 and 0-1 maxima. A plot of $|B + D|^2$ is exhibited in Figure 17 for both the plus and minus signs. Comparison of the excitation profiles with Figure 17 shows that the 1641(dp), 1377(p), 1313(ap), 1005(p), 807(p) and 756(dp) cm^{-1} vibrations are involved in strong non-adiabatic coupling to an electronic state at higher energy. This state is probably V_a .

Vibronic Coupling by Totally Symmetric Modes

Several of the modes listed in the previous section as modes which vibronically couple V and V_a are totally symmetric. Based on a study of vibronic coupling in the cyclic polyene model it has been suggested that a_{1g} modes in porphyrin are not vibronically active in mixing $|Q\rangle$ and $|B\rangle$. In our model the one-electron matrix elements allowing V and V_a to be vibronically coupled (a_{1g}'') are identical to the matrix elements coupling $|Q\rangle$ and $|B\rangle$ in typical metalloporphyrins. Nonetheless, the Band

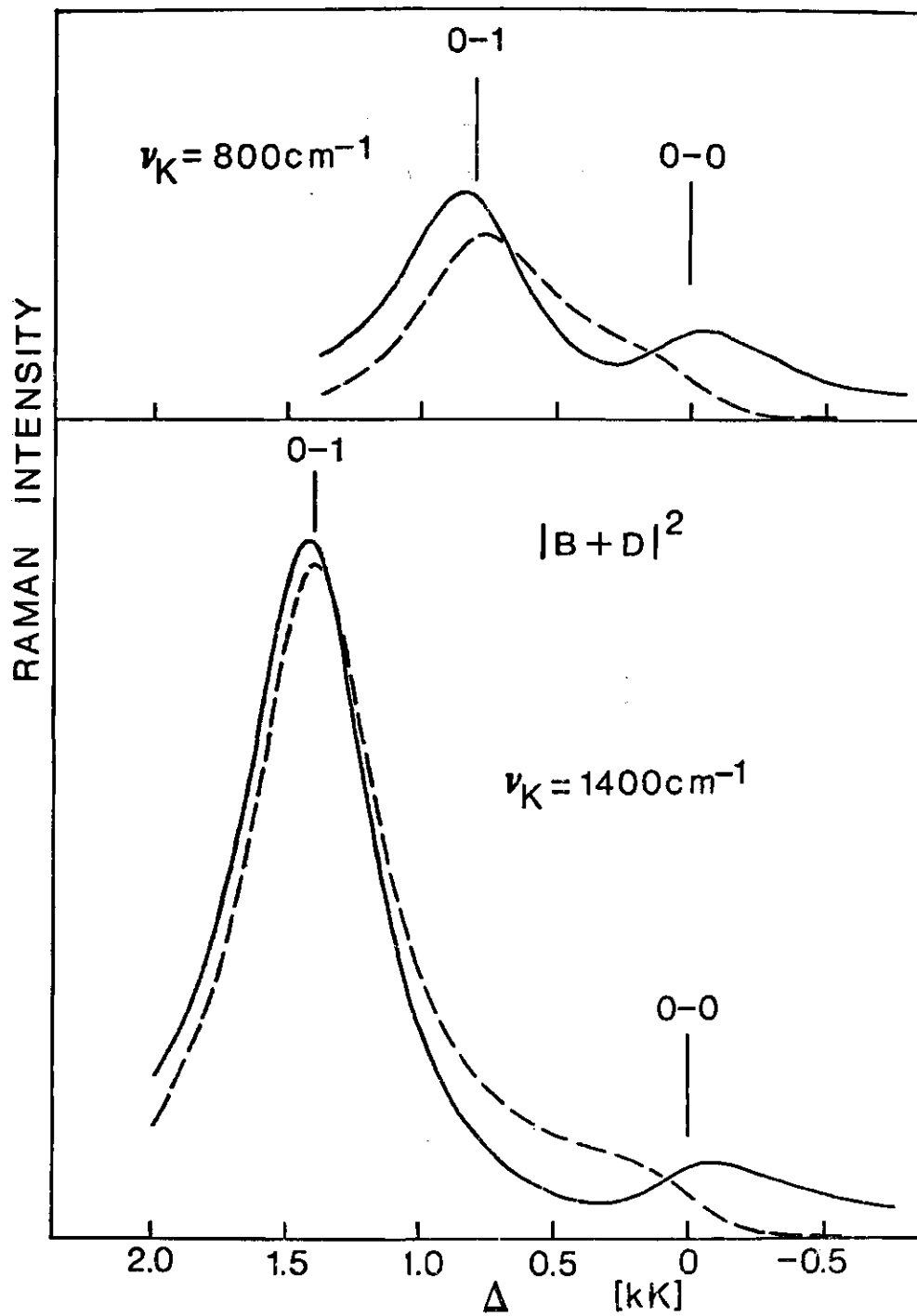


Figure 17. Calculated Raman Intensity When Only B and D Terms Contribute, - - - - Minus Sign, - - - - Plus Sign, $\Delta = E_{V0} - E_{G0} - h\nu$, Compare with Figure 5(B Term Only).

V excitation profiles of the 1377, 1005, and 807 cm^{-1} polarized modes of the NCS^- complex and the 1005(p) cm^{-1} vibration in the I^- complex evidence D term contributions to the Raman scattering. As a consequence it is likely that these vibrations are somewhat active in coupling $|Q\rangle$ and $|B\rangle$ in metalloporphyrins with normal absorption spectra.

The excitation profiles of the 1005(p) cm^{-1} resonance Raman line does not display a pronounced maximum at the 0-0 energy. At first sight this is unexpected since a plus sign for a_{1g} vibrations is anticipated in (56), and a peak should be observed. (Figure 17) It is likely that this vibration which appears in etioporphyrin I, but not in the symmetric octaethylporphyrin⁵⁹ (1025(p) cm^{-1}) involves substantial contribution from the peripheral ethyl and methyl groups. Thus, the proper molecular symmetry now is C_4 and the scattering tensor has no symmetry for symmetric vibrations. Indeed, the depolarization ratio is a function of wavelength and is 0.5 upon laser excitation in the Q band of Cu etioporphyrin I.⁵⁶

On the other hand, a_{1g} modes which do not reflect the reduced symmetry also show vibronic activity in MnEtioNCS. The 807(p) cm^{-1} vibration appears in Ni or Cu octaethylporphyrin⁵⁹ and shifts only slightly in isomers of etioporphyrin.⁶⁰ For this reason, involvement of peripheral groups is presumed small. Nonetheless, the D term is in evidence in the 807 cm^{-1} mode NCS^- complex excitation profile. Similarly, the 1377(p) cm^{-1} mode is vibronically active in the NCS complex; however, some intensity is derived from the A term as has been noted.⁴³

The polarized vibration at 1139 cm^{-1} does not evidence vibronic activity nor does it peak at the anticipated 0-1 frequency but has this maximum shifted to lower frequency. This behavior indicates the excited

state vibrational frequency has changed appreciably from its value in the ground state.

On comparison of the excitation profiles of the 1377(p) cm^{-1} and 807(p) cm^{-1} line in the iodide and thiocyanate complexes, it is observed that the non-adiabatic contribution to the Raman scattering is evident in the thiocyanate excitation profiles but not in the iodide. Inspection of the optical absorption spectra shows that the separation of Band V and V_a is $\sim 2200 \text{ cm}^{-1}$ for the NCS^- complex and $\sim 2700 \text{ cm}^{-1}$ for the iodide complex. Using these values and a 1400 cm^{-1} vibrational frequency, the D term contribution to the Raman scattering (for excitation at the 0-1 frequency) is reduced by a factor of $[(E_{V_a 0} - E_{V1})^{\text{NCS}^-} / (E_{V_a 0} - E_{V1})^{\text{I}^-}]^2 = .38$ for the iodide complex. As a consequence, the non-adiabatic coupling contribution for the I^- complex is insufficient to provide a larger 0-1 maximum in the excitation profile of the 1377 or 807 cm^{-1} lines.

The mechanism⁶¹ by which a totally symmetric mode can couple $|V_a\rangle$ with $|V\rangle$ possibly resides in normal modes which contain pyrrole ring stretching contributions. Consider a bond elongation between the α and β carbon atoms of the pyrrole ring. The electron charge distributions¹ for the pertinent molecular orbitals are shown in Figure 18. Nodes in the $a_{1u}(\pi)$ molecular orbital are through nitrogen and methine bridge carbons, and electron density is high at C_α . Thus $\nu(C_\alpha - C_\beta)$ will modulate the energy of the $a_{1u}(\pi)$ level and mix $|Q\rangle$ and $|B\rangle$ via configuration interaction. Similarly, $\nu(C_\alpha - \text{N})$ will change the orbital energy of $a_{2u}(\pi)$ and $e_g(\pi^*)$, and $\nu(C_\beta - C_\alpha)$ will alter the $e_g(\pi^*)$ energy. A vibrational mode which changes the $a_{1u}(\pi)$ and $a_{2u}(\pi)$ energies in the

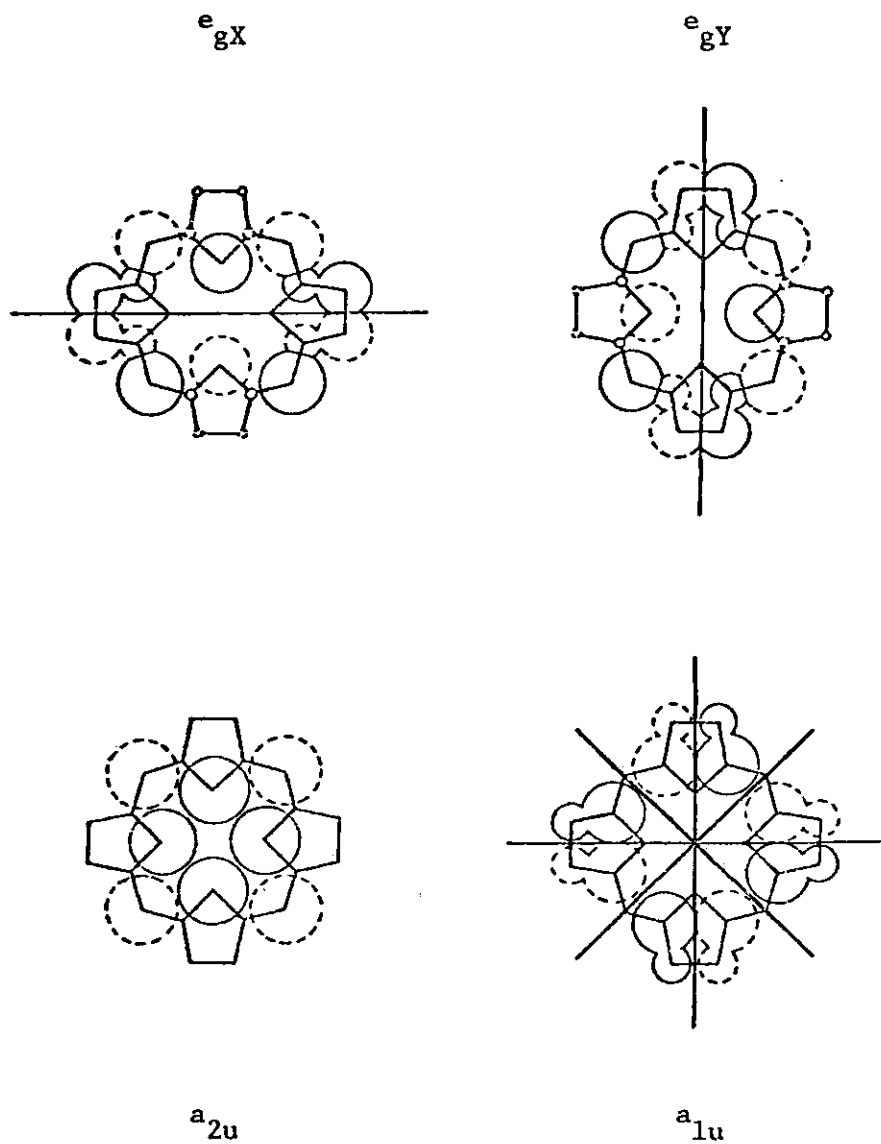


Figure 18. Porphin Molecular Orbitals:³⁹ The Atomic Orbital Coefficients are Proportional to the Size of the Circles; Solid or Dashed Circles Indicate Sign. Symmetry Nodes are Shown.

opposite sense would be most effective in mixing $|B\rangle$ and $|Q\rangle$ (see Table I).

APPENDIX

OUTLINE OF THE THEORY OF RAMAN INTENSITIES

Introduction

In this appendix the theory of Raman intensities is outlined, in particular, the procedure for deriving the transition rates for Raman scattering processes is considered in the framework of second order perturbation theory without damping of states. Damping is included by modifying the results of ~~the perturbation theory~~ in the appropriate way.^{22,26} References are quoted where details have been omitted. The U-matrix formulation⁶² has been employed, since it represents the appropriate starting point for a stochastic treatment of the damping of states problem.¹⁹

Perturbation Theory

The time evolution of the state of a system is determined by the U-matrix (or time evolution operator) defined by,

$$|\psi(t)\rangle = U(t,0)|\psi(0)\rangle, \quad (\text{A-1})$$

and the boundary condition,

$$U(0,0) = 1, \quad (\text{A-2})$$

where $|\psi(t)\rangle$ is the state at time t . In the interaction picture substitution of (A-1) into the Schrodinger equation yields the differential equation for the U-matrix,

$$i\hbar \frac{\partial}{\partial t} U(t,0) = H(t)U(t,0) , \quad (\text{A-3})$$

where $H(t)$ is the hamiltonian describing the perturbing interaction. The solution of this equation can be written in the form of a sum of successive approximations,¹⁹

$$U(t,0) = \sum_{k=0} U_k(t,0) \quad (\text{A-4})$$

where $U_0(t,0) \equiv 1$, and ($k \neq 0$)

$$U_k(t,0) = (-i/\hbar)^k \int_0^t dt_k \int_0^{t_k} dt_{k-1} \dots \int_0^{t_2} dt_1 H(t_k)H(t_{k-1}) \dots H(t_1) \quad (\text{A-5})$$

For the problem at hand, we will consider the non-interacting molecule and radiation field as the unperturbed system; the perturbing hamiltonian describes the interaction between the radiation field and the electrons of the polyatomic molecule. (We will neglect the interaction between the nuclei and the radiation field.)

The Interaction Matrix Elements

The interaction between the radiation field and a polyatomic molecule⁶² is described by the hamiltonian

$$H = H^{(1)} + H^{(2)} , \quad (\text{A-6})$$

where

$$H^{(1)} = \frac{e}{m} \sum_k \vec{p}_k \cdot \vec{A}(\vec{r}_k) , \quad (\text{A-7})$$

and

$$H^{(2)} = \frac{e^2}{2mc^2} \sum_{\mathbf{k}} \vec{A}^2(\vec{r}_{\mathbf{k}}), \quad (\text{A-8})$$

where e , m , and $\vec{p}_{\mathbf{k}}$ are, respectively, the charge, mass, and momentum operator of the \mathbf{k}^{th} electron, and $\vec{A}(\vec{r}_{\mathbf{k}})$ is the vector potential operator at the position of the \mathbf{k}^{th} electron. $\vec{A}(\vec{r}_{\mathbf{k}})$ is expressible as a linear combination of creation and annihilation operators for each mode of the field.

The unperturbed states are products of the exact molecular eigenstates $|i\rangle$ and the radiation field states $|\dots m_{\nu} \dots\rangle$ where m_{ν} is the occupation number of the ν^{th} mode of the radiation field. With these unperturbed states specified the matrix elements of the interaction hamiltonian (A-6) can be obtained using standard procedures for evaluating the photon matrix elements. The following matrix elements of $H^{(1)}$ (in the Schrodinger picture) are required.¹⁹

$$H_{i, m_{\nu}-1; j, m_{\nu}}^{\nu} \equiv \langle i; \dots, m_{\nu}-1, \dots | H^{(1)} | j; \dots, m_{\nu}, \dots \rangle \quad (\text{A-9})$$

and

$$= \langle i | -\frac{e}{m} \sqrt{\frac{2\pi\hbar m_{\nu}}{V\omega_{\nu}}} \sum_{\mathbf{k}} e^{-i\vec{k}_{\nu} \cdot \vec{r}_{\mathbf{k}}} \hat{\mathbf{e}}_{\nu, \vec{p}_{\mathbf{k}}} | j \rangle \quad (\text{A-9})$$

and

$$H_{i, m_{\nu}+1; j, m_{\nu}}^{\nu} \equiv \langle i; \dots, m_{\nu}+1, \dots | H^{(1)} | j; \dots, m_{\nu}, \dots \rangle \quad (\text{A-10})$$

$$= \langle i | -\frac{e}{m} \sqrt{\frac{2\pi\hbar (m_{\nu}+1)}{V\omega_{\nu}}} \sum_{\mathbf{k}} e^{-i\vec{k}_{\nu} \cdot \vec{r}_{\mathbf{k}}} \hat{\mathbf{e}}_{\nu, \vec{p}_{\mathbf{k}}} | j \rangle$$

where the volume V is included for normalization. $|\vec{k}_\nu| = \frac{\omega_\nu}{c}$, and ω_ν and \hat{e}_ν are the angular frequency and polarization unit vector, respectively, of a photon of the ν^{th} mode of the radiation field.

The Transition Probabilities

The probability of a transition from the unperturbed state $|\beta\rangle$ to the state $|\alpha\rangle$ by time t is given by

$$W_{\alpha\beta} = |U_{\alpha\beta}^{(1)}(t,0)|^2 = |\langle\alpha|U(t,0)|\beta\rangle|^2. \quad (\text{A-11})$$

We are interested in two photon processes, i. e., transitions in which a photon of mode μ is created and one of mode ν is destroyed. Remembering that $H^{(1)}$ is linear in the creation and destruction operators, whereas $H^{(2)}$ is bilinear, equations (A-4) and (A-5) give ($\alpha \neq \beta$)

$$U_{\alpha\beta}(t,0) = H_{\alpha\beta}^{(2)} \frac{1 - e^{i(E_\alpha - E_\beta)t/\hbar}}{E_\alpha - E_\beta} \quad (\text{A-12})$$

$$+ \sum_{\eta \neq \alpha, \beta} \frac{H_{\alpha\eta}^{(1)} H_{\eta\beta}^{(1)}}{E_\eta - E_\beta} \left[\frac{1 - e^{i(E_\alpha - E_\eta)t/\hbar}}{E_\alpha - E_\eta} - \frac{1 - e^{i(E_\alpha - E_\beta)t/\hbar}}{E_\alpha - E_\beta} \right]$$

to second order in the interaction hamiltonian (A-1).

The Raman Scattering Tensor and Transition Rates

We now outline the procedure by which (A-12) leads to the Raman intensity in terms of the scattering tensor. In the following let the states $|\alpha\rangle$ and $|\beta\rangle$ in (A-12) be $|n'; \dots, m_\nu - 1, \dots, m_\mu + 1, \dots\rangle$ and

$|n; \dots, m_\nu, \dots, m_\mu, \dots\rangle$, respectively. The steps in the procedure for obtaining the fundamental expressions ((A-17) and (A-18)) for Raman scattering are: (1) Making the dipole approximation, we set $e^{-i\vec{k}_\nu \cdot \vec{r}_{k=1}}$, since $kr \ll 1$ for typical electron displacements in the molecule and optical photon wavelengths. As a consequence, the first term in (A-12) vanishes except for Rayleigh scattering, that is, due to the orthogonality of the exact molecular eigenstates the matrix elements of $H^{(2)}$ (see reference 26) vanish for $n \neq n'$. (2) Damping of states can be included by the damping operator method,²⁶ the result can be obtained here by replacing the energy of the molecular state E_i by the complex energy $E_i - i\Gamma_i$, where Γ_i is the half-width of the quasistationary molecular state $|i\rangle$. In addition the whole expression is multiplied by $e^{-i\Gamma_n t/\hbar}$ (where Γ_n is the damping coefficient for the final molecular eigenstate). (3) The first term in the brackets can be shown³⁰ to vanish for excitation into a continuum, i. e. transient effects are negligible. (4) The sum over photon states in (A-12) gives two terms--one for each time ordering of the creation and annihilation of the photons of modes μ and ν .

Steps (1)-(4) and evaluation of the matrix elements using (A-9) and (A-10) give,

$$\begin{aligned}
 U_{n', m_\nu - 1, m_\mu + 1; n, m_\nu, m_\mu}(t, 0) = & \frac{2\pi\hbar e^2}{V m^2} \sqrt{\frac{(m_\mu + 1)m_\nu}{\omega_\nu \omega_\mu}} \sum_{i \neq n, n'} \left[\frac{\langle n' | \hat{e}_\nu \cdot \vec{P} | i \rangle \langle i | \hat{e}_\mu \cdot \vec{P} | n \rangle}{E_i - E_n + \hbar\omega_\mu - i(\Gamma_i - \Gamma_n)} \right. \\
 & \left. + \frac{\langle n' | \hat{e}_\mu \cdot \vec{P} | i \rangle \langle i | \hat{e}_\nu \cdot \vec{P} | n \rangle}{E_i - E_n - \hbar\omega_\nu - i(\Gamma_i - \Gamma_n)} \right] \quad (A-13)
 \end{aligned}$$

$$\times \left[e^{-\Gamma_n t/\hbar} \frac{e^{i[E_n - E_n - \hbar(\omega_\nu - \omega_\mu) - i(\Gamma_n - \Gamma_n)]t/\hbar}}{E_n - E_n - \hbar(\omega_\nu - \omega_\mu) - i(\Gamma_n - \Gamma_n)} \right]$$

where $\vec{P} \equiv \sum_k \vec{p}_k$. Conventionally, Γ_n and Γ_n are assumed²⁶ to vanish for the Raman scattering process (since they represent the widths of vibronic levels of the ground electronic state which are presumed small). (5) In the next step the transition rate is derived from the transition probabilities (A-11) according to

$$\bar{w}_{\alpha\beta} \equiv \frac{d}{dt} \bar{W}_{\alpha\beta}(t) = \frac{d}{dt} |U_{\alpha\beta}(t,0)|^2. \quad (A-14)$$

Substituting (A-13) into (A-14), the transition rate for excitation into a continuum in the dipole approximation is, setting $\hat{e}_\nu = \hat{e}_\mu = \hat{e}$, $\omega_\nu = \omega$, $\hat{e}_\mu = \hat{e}'$,

$$\begin{aligned} \dot{w}_{n',n} = & \frac{8\pi^3 \hbar e^4 m(m'+1)}{V^2 m^4 \omega \omega'} \left| \sum_{i \neq n, n'} \left[\frac{\langle n' | \hat{e}' \cdot \vec{P} | i \rangle \langle i | \hat{e} \cdot \vec{P} | n \rangle}{E_i - E_n + \hbar\omega - i\Gamma_i} \right. \right. \\ & \left. \left. + \frac{\langle n' | \hat{e}' \cdot \vec{P} | i \rangle \langle i | \hat{e} \cdot \vec{P} | n \rangle}{E_i - E_n - \hbar\omega - i\Gamma_i} \right] \right|^2 \delta(E_n' - E_n - \hbar(\omega - \omega')) \end{aligned} \quad (A-15)$$

where energy conservation provided by the δ -function has been used in writing the denominator in the first term in terms of ω . (6) The next step is to employ $[\vec{x}_k, H] = i\hbar \frac{\delta H}{\delta \vec{p}_k}$ to obtain,

$$\frac{e}{m} \langle i | \hat{e}' \cdot \vec{p}_k | j \rangle = -i\omega' \langle i | \hat{e}' \cdot e\vec{r}_k | j \rangle. \quad (A-16)$$

In terms of the dipole matrix elements, the transition rate is written as,

$$\dot{w}_{n',n} = \frac{8\pi^3 \hbar m(m'+1)\omega\omega'}{V^2} \left| \sum_{\rho,\sigma} e_{\rho} R_{\rho\sigma} e'_{\sigma} \right|^2 \delta(E_n - E_{n'} - \hbar(\omega - \omega')), \quad (\text{A-17})$$

where $R_{\rho\sigma}$ is the scattering tensor defined by,

$$R_{\rho\sigma} = \sum_{i \neq n, n'} \left[\frac{\langle n' | R_{\rho} | i \rangle \langle i | R_{\sigma} | n \rangle}{E_i - E_{n'} + \hbar\omega - i\Gamma_i} + \frac{\langle n' | R_{\sigma} | i \rangle \langle i | R_{\rho} | n \rangle}{E_i - E_n - \hbar\omega - i\Gamma_i} \right], \quad (\text{A-18})$$

and e_{ρ} and e'_{σ} are the components of the unit polarization vectors in the molecular coordinates X, Y, and Z. (7) The expression for spontaneous ($m'=0$) Raman intensity of light scattered into the element of solid angle $d\Omega'$ and the frequency interval $[\omega', \omega' + d\omega']$ results²⁶ on multiplying the transition rate by the number of photon states in the neighborhood of ω', e' , i.e. $\rho(\omega') d\omega' d\Omega' = \frac{\omega'^2 V}{(2\pi c)^3} d\omega' d\Omega'$. (The incident light frequency and angular distribution must also be taken into account).

Finally, the expression is multiplied by the energy of the scattered photon $\hbar\omega'$. If randomly oriented molecules are to be studied, the standard scattering geometry can be assumed, and equation (A-17) averaged over the molecular orientations relative to the laboratory-fixed polarization and direction of propagation.¹⁵

BIBLIOGRAPHY

1. M. Gouterman, *J. Mol. Spectrosc.*, 6, 138 (1961).
2. C. Weiss, H. Kobayashi, M. Gouterman, *J. Mol. Spectrosc.*, 16, 415 (1965).
3. M. Gouterman, *J. Chem. Phys.*, 30, 1139 (1959).
4. M. Gouterman, G. H. Wagniere, L. C. Snyder, *J. Mol. Spectrosc.*, 11, 108 (1963).
5. W. Caughey, R. Deal, C. Weiss, and M. Gouterman, *J. Mol. Spectrosc.*, 16, 451 (1965).
6. H. Kobayashi, *J. Chem. Phys.* 30, 1362 (1959).
7. R. R. Gaughan, D. F. Shriver, and L. J. Boucher, *Proc. Natl. Acad. Sci.*, 72, 433 (1975).
8. L. J. Boucher, *Coord. Chem. Revs.*, 7, 289 (1972).
9. L. J. Boucher, *Ann. N.Y. Acad. Sci.*, 205, 409 (1973).
10. M. Mingardi and W. Siebrand, *J. Chem. Phys.*, 62, 1074 (1975).
11. M. Gouterman, L. K. Hanson, G. E. Khalil, and W. R. Leenstra, *J. Chem. Phys.*, 62, 2343 (1975).
12. H. A. Kramers and W. Heisenberg, *Z. Physik*, 31, 681 (1925).
13. P. A. M. Dirac, *Proc. Roy. Soc. (London)*, 114, 710 (1927).
14. J. H. Van Vleck, *Proc. Natl. Acad. Sci. U.S.*, 15, 754 (1929).
15. G. Placzek, in "Handbuch der Radiologie," E. Marx, Ed., (Akademische Verlagsgesellschaft, Leipzig), Vol. 6, 205 (1934); English trans. by A. Werbin, UCRL Trans-526(L), is processed by the clearing house for Federal Scientific and Technical Information of the U.S. Department of Commerce.
16. A. C. Albrecht, *J. Chem. Phys.* 34, 1476 (1961).
17. J. Tang and A. C. Albrecht, in "Raman Spectroscopy," H. A. Szymanski, Ed. (Plenum Press, Inc., New York) Vol. 2, 33 (1970).

BIBLIOGRAPHY (Continued)

18. G. Herzberg and E. Teller, *Z. Physik Chem.*, B21, 410 (1933).
19. J. Behringer, in "Molecular Spectroscopy," R. F. Barrow, D. A. Long, and D. J. Millen, Eds., Vol. 2, The Chemical Society, London, 100 (1974).
20. H.-K. Hong, *Chem. Phys.*, 9, 1 (1975).
21. V. Weisskopf and E. Wigner, *Z. Physik*, 63, 54 (1930); 65, 18 (1930).
22. W. Heitler, "The Quantum Theory of Radiation," (Clarendon Press, Oxford), 3 edn., 1954.
23. M. Jacon, R. Germinet, M. Berjot, and L. Bernard, *J. Phys. Radium*, 32, 517 (1971).
24. M. Jacon, in "Advances in Raman Spectroscopy," J.-P. Mathieu, Ed., (Heyden and Son, London), Vol. 1, 325 (1973).
25. A Messiah, "Quantum Mechanics," (North-Holland Publishing Company, Amsterdam), Vol. 2, 1965.
26. M. M. Sushchinskii, "Raman Spectra of Molecules and Crystals," (Israel Program for Scientific Translations, New York), 1972.
27. J. A. Shelnutz, unpublished work.
28. R. F. Fox, *J. Math. Phys.*, 13, 1196 (1972).
29. G. Wentzel, in "Handbuch der Physik," H. Geiger and K. Scheel, (Springer, Berlin), Vol. 24, 695 (1933).
30. J. Behringer, *J. Raman Spectrosc.*, 2, 275 (1974).
31. M. Born and R. Oppenheimer, *Ann. Physik*, 87, 457 (1927).
32. M. Bixon and J. Jortner, *J. Chem. Phys.*, 48, 715 (1968).
33. A. C. Albrecht, *J. Chem. Phys.*, 33, 156 (1960).
34. G. Orlandi and W. Siebrand, *J. Chem. Phys.*, 58, 4513 (1968).
35. L. A. Nafie and W. L. Peticolas, to be published.
36. W. L. Peticolas, L. Nafie, P. Stein, and B. Fanconi, *J. Chem. Phys.*, 52, 1576 (1970).

BIBLIOGRAPHY (Continued)

37. J. E. Falk, in BBA Library, "Porphyrins and Metalloporphyrins," (Elsevier Publishing Company, Amsterdam), Vol. 2, 1964.
38. R. E. Linder, G. Barth, E. Bunnenberg, C. Dyerassi, L. Seamans, and A. Moscovitz, J. Chem. Soc. Perkin II, 1712 (1974).
39. H. C. Longuet-Higgins, C. W. Rector, and J. R. Platt, J. Chem. Phys., 13, 1174 (1950).
40. M. H. Perrin, M. Gouterman, and C. L. Perrin, J. Chem. Phys., 50, 4137 (1969).
41. M. Tinkham, "Group Theory and Quantum Mechanics," (McGraw-Hill Book Company, New York), 1964.
42. L. A. Nafie, M. Pezolet, and W. L. Peticolas, Chem. Phys. Lett., 20, 563 (1973).
43. T. C. Strekas, A. J. Packer, and T. G. Spiro, J. Raman Spectrosc., 1, 197 (1973).
44. F. Galluzzi, M. Garozzo, and F. F. Ricci, J. Raman Spectrosc., 2, 351 (1974).
45. J. A. Koningstein and B. G. Jakubinek, J. Raman Spectrosc., 2, 317 (1974).
46. M. M. McClain, J. Chem. Phys., 55, 2789 (1971).
47. J. Friedman and R. Hochstrasser, Chem. Phys. Lett., 32, 414 (1975).
48. T. G. Spiro and T. C. Strekas, Proc. Nat. Acad. Sci. U.S., 69, 2622 (1972).
49. F. Inagaki, M. Tasumi, and T. Miyazawa, J. Mol. Spectrosc., 50, 286 (1974).
50. M. Zerner and M. Gouterman, Theoret. Chim. Acta. (Berlin), 4, 44 (1966).
51. M. Abe, T. Kitigawa, and Y. Kyogoku, (private communication).
52. H. Ogoshi, E. Watanabe, F. Yoshida, J. Kincaid, and K. Nakamoto, J. Amer. Chem. Soc., 95, 2845 (1973).
53. T. C. Strekas, D. H. Adams, A. Packer, T. G. Spiro, Appl. Spectrosc., 28, 324 (1974).

BIBLIOGRAPHY (Continued)

54. H. Hamaguchi, I. Harada, and T. Shimanouchi, Chem. Lett. (Japan), 1405 (1974).
55. A. L. Verma, R. Mendelsohn, and H. J. Bernstein, J. Chem. Phys., 61, 383 (1974).
56. R. Mendelsohn, S. Sunder, A. L. Verma, and H. J. Bernstein, J. Chem. Phys., 62, 37 (1975).
57. H. Kobayashi, M. Shimizu, and F. Fujita, Bull. Chem. Soc. Japan, 43, 2335 (1970).
58. G. J. Small and E. S. Yeung, Chem. Phys., 9, 379 (1975).
59. L. D. Spaulding, C. C. Chang, N. T. Yu, and R. H. Felton, J. Amer. Chem. Soc., 97, 2517 (1975).
60. S. Sunder, R. Mendelsohn, and H. J. Bernstein, Biochem. Biophys. Res. Comm., 62, 12 (1975).
61. M. Gouterman, (private communication).
62. J. J. Sakurai, ~~Advanced Quantum Mechanics~~, Addison-Wesely Publ. Co., (1967).

VITA

I was born in Bremen, Georgia on March 9, 1946, the son of George and Zettie Shelnutt. Upon graduation from Bremen High School, I entered Georgia Tech in the Summer of 1964, receiving a Bachelor of Science in Physics in 1968. I was employed by the Naval Weapon Center for two years. I then entered the Physics graduate program and received a Master of Science in September, 1971, and a Doctor of Philosophy in December, 1975. As a graduate student I was supported by teaching and research assistantships and a National Science Foundation Traineeship.

VITA

I was born in Bremen, Georgia on March 9, 1946, the son of George and Zettie Shelnutt. Upon graduation from Bremen High School, I entered Georgia Tech in the Summer of 1964, receiving a Bachelor of Science in Physics in 1968. I was employed by the Naval Weapon Center for two years. I then entered the Physics graduate program and received a Master of Science in September, 1971, and a Doctor of Philosophy in December, 1975. As a graduate student I was supported by teaching and research assistantships and a National Science Foundation Traineeship.